AD NUMBER
AD319643
CLASSIFICATION CHANGES
TO: **UNCLASSIFIED**
FROM: **CONFIDENTIAL**
LIMITATION CHANGES
TO: **Approved for public release; distribution is unlimited.**
FROM: **Distribution authorized to U.S. Gov't. agencies and their contractors; Administrative/Operational Use; SEP 1960. Other requests shall be referred to Office of Naval Research, Arlington, VA 22203.**
AUTHORITY
ONR ltr 28 Jul 1977 ; ONR ltr 28 Jul 1977

NOX

MASSACHUSETTS INSTITUTE OF TECHNOLOGY
NAVAL SUPERSONIC LABORATORY

Technical Report 307

(UNCLASSIFIED TITLE)

CORRELATION TECHNIQUES FOR INFRARED DETECTION SYSTEMS

by

Terence J. Wieting

September 1960

MASSACHUSETTTS INSTITUTE OF TECHNOLOGY
Naval Supersonic Laboratory

Technical Report 307

(UNCLASSIFIED TITLE)

CORRELATION TECHNIQUES FOR INFRARED DETECTION SYSTEMS

by

Terence J. Wieting

Contract Nonr 1841(40)
Contract AF 33(616)-6046
MITRE Subcontract No. 27
M.I.T. DSR 8150 and 8170

September 1960

This report contains viii
and 56 pages. Copy No. 32
of 100 copies.
NSL 3711

FOREWORD

This work was performed in whole or in part under the combined support of the Department of the Navy's Office of Naval Research and Bureau of Weapons [Contract Nonr 1841(40)], the Weapons Guidance Laboratory of the United States Air Force's Wright Air Development Division [Contract AF 33(616)-6046], and the MITRE Corporation under Subcontract No. 27.

ABSTRACT

Correlation techniques can be applied to infrared detection systems to improve the signal-to-noise ratio of the radiation detector. Two such correlation systems are compared and evaluated; (1) a single detector synchronous rectification system, and (2) a two-detector cross-correlation system. The two systems are interpreted in the context of search and tracking operations, and a discussion of the transfer of target information through these systems is presented. An experimental study verifying the theoretical analysis of the two-detector cross-correlation system has been carried out.

TABLE OF CONTENTS

LIST OF ILLUSTRATIONS

TABLE OF CONTENTS Concluded

SYMBOLS

$Ci(x)$	Defined by Equation (4.25)
E	True signal component contained in S
$e(t)$	True signal component contained in s
$e'(t)$	Reference signal waveform
f	Frequency; bandwidth limits
f_0	Target signal frequency
Δf	Bandwidth of the noise, $\Delta \nu(t)$
Δf^*	Equivalent noise bandwidth (defined by Equation 2.20)
N	rms value of $\Delta N(t)$
ΔN	Noise component contained in S
$P(f)$	Power spectrum of $\Delta \nu(t)$
P_{max}	Maximum value of P(f)
$p(f)$	Amplitude-normalized power spectrum of $\Delta \nu(t)$
$Q(T)$	Improvement in signal-to-noise ratio (defined by Equation 4.11)
$Q^*(T)$	Improvement in signal-to-noise ratio for unit bandwidth
R_0	Unit-impulse response function
S	Correlator output signal
$Si(x)$	Defined by Equation (4.8)
s	Signal from radiation detector entering correlator
T	Integration time
t	Time
$W_i(f)$	Transfer function of integrator network
γ	A constant equal to 1.781
Δ	Root-mean-square fractional error in Q(T)
δ	Dirac delta function
ε	Amplitude of sinusoidal target signal
ε'	Amplitude of sinusoidal reference signal
$\theta(T)$	Defined on pp. 8, 11, and 12 with various subscripts
ν	rms value of $\Delta \nu(t)$
$\Delta \nu$	Noise component contained in s
τ	Time, as distinguished from t

SYMBOLS (Concluded)

$\Phi(f)$	Noise power spectrum
$\Psi(\tau)$	Autocorrelation function
$\psi(\tau)$	Autocorrelation function of $\Delta\nu(t)$
$\psi'(\tau)$	Autocorrelation function of $e'(t)$

I. INTRODUCTION

In the past decade a number of technical reports have been written on the uses and applications of the correlation function. The foundation for this development was laid by Wiener[1] in 1930 with the introduction of the correlation function and its Fourier transform, the power spectrum. Applications have been made in such diverse fields as astronomy (Ref. 2, pp. 120-126), biophysics,[3] and infrared physics.[4]

One of the most promising applications of the correlation function is in the detection of signals in random noise. The initial papers of Lee and Wiesner[5] (1950) and Lee, Cheatham, and Wiesner[6] (1950) present a discussion of the autocorrelation and cross-correlation methods for the detection of signals in noise. A somewhat amplified version of this work has been done by Fano[7] (1951) and Davenport[8] (1951). A mathematical analysis of the Dicke[9] radiometer together with another system using two independent receivers has been carried out by Goldstein[10] (1955). Still more recently Jacobson[11] (1957) has examined a multiple receiver system, laying primary emphasis upon obtaining directional information from the received signal. In addition to the above, the Massachusetts Institute of Technology (MIT) Research Laboratory of Electronics (RLE) has published several progress reports (e.g., Refs. 12–14) dealing with correlators and their use in the detection of signals below the noise level.

The relationship between the use of correlation techniques and optimum filter techniques is one of domain. The original work of North[15] (1943) and Van Vleck and Middleton[16] (1946) in the theory of

---

[1] Superscripts refer to References

optimum filters is reviewed in a paper by Zadeh and Raggazzini[17] (1952). Also appearing in this paper is a discussion of the relationship between correlation techniques and optimum filter techniques. Theoretically, no claim to superiority can be made for either method, inasmuch as stationary random noise contains the same information whether described in the frequency domain (power spectrum) or time domain (autocorrelation function). However, from a practical point of view, the operation of a system in the time domain may be more feasible for many applications. Comments to this effect may be found in Ref. 6.

The purpose of this report is two-fold. The first part is a theoretical analysis of two detection systems, the synchronous rectification system and the two-detector cross-correlation system. The function of these systems is to improve the signal-to-noise ratio of radiation detectors. The analysis followed in the above references (viz. 5–11) is generalized; particular attention is paid to the effect which the form of the power spectrum has upon the improvement in the signal-to-noise ratio. Each system is then interpreted in the context of the current infrared systems being used for search and tracking operations. The second part is an experimental confirmation of the two-detector cross-correlation system by means of a correlator developed at the MIT Naval Supersonic Laboratory (NSL).

II. THE SYNCHRONOUS RECTIFICATION SYSTEM

A block diagram of this system is shown in Figure 1. The signal and noise waveforms included in the diagram indicate the successive operations which improve the signal-to-noise ratio of the radiation detector. For convenience, the target signal is shown as a sinusoid. Radiation from a target -- after passing through the chopper -- falls on the detector and is sent to the preamplifier, appearing in the output as the waveform indicated in Figure 1. A reference signal of the same frequency and phase as the target signal is produced by a steady light source and detector combination. The noise in the reference-signal waveform is assumed to be negligibly small. The two waveforms are subsequently multiplied together and then integrated; the result being that the target signal will increase at a more rapid rate with time than the root-mean-square noise. The combined operations of multiplication and integration (or averaging) are called cross-correlation.

The system indicated in Figure 1 may have several alternative forms. For instance, the multiplier can be replaced by a phase-sensitive detector. The function of the phase-sensitive detector is simply to reverse the sign of all waveforms during the negative phase of the reference waveform, and pass all waveforms unchanged during the positive phase of the reference waveform.

Before proceeding with the analysis a few definitions must be made. The output of the radiation detector before entering the correlator will be written as

$$s(t) = e(t) + \Delta\nu(t) \quad , \qquad (2.1)$$

where $e(t)$ and $\Delta\nu(t)$ are the true signal and noise components, respectively. The output of the integrator can then be written as

$$S(t) = \int_0^T s(t)\, e'(t) dt \quad , \tag{2.2}$$

where e'(t) is the reference signal waveform entering the correlator. Expanding (2.2), it follows that

$$S(t) = \int_0^T e(t)\, e'(t) dt + \int_0^T \Delta\nu(t)\, e'(t)\, dt \tag{2.3}$$

The first term of (2.3) is the signal component in the output of the integrator.

$$E(T) \equiv \int_0^T e(t)\, e'(t)\, dt \tag{2.4}$$

The second term of (2.3) is the noise component in the output of the integrator.

An evaluation of the second term of (2.3) requires that some of the properties of the noise $\Delta\nu(t)$ be known. We shall assume that the cell noise, photon noise, and circuit noise comprising $\Delta\nu(t)$ have the following general properties:

a) Stationarity, $\overline{\Delta\nu(t)^2} = \overline{\Delta\nu(t \pm t_0)^2}$ for all t_0

b) $\overline{\langle \Delta\nu(t)^2 \rangle_T} = \langle \overline{\Delta\nu(t)^2} \rangle_T$

c) Ergodicity, $\lim_{T \to \infty} \langle \Delta\nu(t)^2 \rangle_T = \overline{\Delta\nu(t)^2}$.

The brackets denote a time average over the period T, whereas the bar indicates an ensemble (statistical) average. No attempt to justify the above properties will be made. The assumptions are not unduly restrictive, and the experimental data obtained on the basis of these assumptions substantially confirm their correctness. A discussion of the above properties may be found in Reference 18 together with appropriate source material.

It is well known that the output of a linear network can be expressed by the equation

$$\Delta N(t) = \int_{-\infty}^{\infty} \Delta n(\tau) R_0 (t - \tau)\, d\tau \quad , \tag{2.5}$$

where $\Delta n(\tau)$ is the input waveform to the linear network and $R_0 (t - \tau)$ is the unit-impulse response function of the network. This equation can be verified by a simple application of the Fourier integral theorem. To find the statistical mean-square value of $\Delta N(t)$ we make the following operations:

$$\Delta N(t)^2 = \int_{-\infty}^{\infty} \Delta n(\tau) R_0(t - \tau)\, d\tau \int_{-\infty}^{\infty} \Delta n(\tau') R_0 (t - \tau')\, d\tau' \quad , \tag{2.6}$$

$$\Delta N(t)^2 = \int_{-\infty}^{\infty} \int_{-\infty}^{\infty} \Delta n(\tau) \Delta n(\tau') R_0 (t - \tau) R_0 (t - \tau')\, d\tau\, d\tau' \quad , \tag{2.7}$$

where τ' is introduced to distinguish the two independent integrations. Taking the statistical average of (2.7) and making use of property b) above, we have

$$\overline{\Delta N(t)^2} = \int_{-\infty}^{\infty} \int_{-\infty}^{\infty} \overline{\Delta n(\tau) \Delta n(\tau')}\, R_0 (t - \tau) R_0 (t - \tau')\, d\tau\, d\tau' \quad . \tag{2.8}$$

The stationarity property permits us to equate $\overline{\Delta n(\tau) \Delta n(\tau')}$ with the autocovariance function $\Psi(\tau - \tau')$ of the noise $\Delta n(\tau)$; that is,

$$\overline{\Delta N(t)^2} = \int_{-\infty}^{\infty} \int_{-\infty}^{\infty} \Psi(\tau - \tau') R_0 (t - \tau) R_0 (t - \tau') d\tau\, d\tau' \quad . \tag{2.9}$$

The ergodic property implies the equality of the autocovariance and autocorrelation functions. Moreover, since the power spectrum of a random process is defined as the Fourier transform of the autocorrelation function, we may write

$$\Psi(\tau - \tau') = \int_{-\infty}^{\infty} \Phi (f) \cos 2\pi f(\tau - \tau')\, df \tag{2.10}$$

Equations (2.9) and (2.10) require only that the power spectrum of the noise and the unit-impulse response function be known in order

to obtain the mean-square noise in the output of the network.

The autocovariance function of a stationary random process, e.g. u(t), is defined by the equation

$$\Psi(\tau) = \overline{u(t)\,u(t+\tau)} \tag{2.11}$$

where the bar denotes an ensemble average. Some of the properties of the autocovariance function include the following:

$$\Psi(\tau) = \Psi(-\tau) \tag{2.12}$$

and

$$\Psi(\tau) \leq \Psi(0) = \overline{u^2} \quad , \tag{2.13}$$

where $\overline{u^2}$ is the ensemble mean-square value of u(t). The autocorrelation function is defined by

$$\Psi(\tau) = \lim_{T\to\infty} \frac{1}{2T} \int_{-T}^{T} u(t)u(t+\tau)\,dt \tag{2.14}$$

In view of the ergodic property already assumed, the autocorrelation and autocovariance functions are equivalent.

The unit-impulse response function of the integrator network of (2.3) is

$$R_0(t-\tau) = \int_0^T \delta(t-\tau)dt \quad , \tag{2.15}$$

where $\delta(t-\tau)$ is the Dirac delta function. Equation (2.15) is very easily evaluated to give

$$R_0(t-\tau) = \begin{cases} 1 & , \ 0 \leq \tau \leq T \\ 0 & , \ \tau > T \text{ or } \tau < 0 \end{cases} \quad . \tag{2.16}$$

Inserting (2.10) and (2.16) into (2.9) and carrying out the two integrals in τ and τ' gives

$$\overline{\Delta N^2} = \frac{1}{2\pi^2} \int_{-\infty}^{\infty} \frac{\Phi(f)\,(1-\cos 2\pi f T)\,df}{f^2} \quad . \tag{2.17}$$

The form of the power spectrum $\Phi(f)$ depends upon the power spectrums (or autocorrelation functions) of the signals entering the multiplier and the transfer function of the multiplier.

Since the two functions in the second term of (2.3) are independent, the autocorrelation function of the product $\Delta\nu(t)e'(t)$ can be written as

$$\Psi(\tau) = \psi(\tau)\ \psi'(\tau) \quad , \tag{2.18}$$

where $\psi(\tau)$ and $\psi'(\tau)$ are the autocorrelation functions of $\Delta\nu(t)$ and $e'(t)$, respectively. Using the fundamental theorem that the autocorrelation function and the power spectrum constitute a Fourier transform pair (see Eq. (2.10)) the power spectrum associated with $\Psi(\tau)$ can be written as

$$\Phi(f) = \int_{-\infty}^{\infty} \left\{ \int_{-\infty}^{\infty} P(f) \cos 2\pi f\tau \, df \right\} \psi'(\tau) \cos 2\pi f\tau \, d\tau \quad , \tag{2.19}$$

where $P(f)$ is the power spectrum of $\Delta\nu(t)$. For convenience a noise equivalent bandwidth will be defined as follows:

$$\Delta f^* \equiv \int_{-\infty}^{\infty} p(f)\, df \quad , \tag{2.20}$$

where

$$p(f) = \frac{P(f)}{P_{max}} \quad . \tag{2.21}$$

In addition the mean-square value of $\Delta\nu(t)$ will be written as

$$\nu^2 = \int_{-\infty}^{\infty} P(f)\, df = P_{max}\ \Delta f^* \quad . \tag{2.22}$$

Inserting (2.19) into (2.17) and using the results of (2.20) and (2.22), the mean square noise in the output of the integrator becomes

$$\overline{\Delta N^2} = \frac{\nu^2}{2\pi^2}\,\theta\,(T) \quad , \tag{2.23}$$

where

$$\theta(T) \equiv \frac{\int_{-\infty}^{\infty}\left\{\int_{-\infty}^{\infty}\psi'(\tau)\cos 2\pi f\tau\left[\int_{-\infty}^{\infty}p(f)\cos 2\pi f\tau\,df\right]d\tau\right\}\frac{(1-\cos 2\pi fT)}{f^2}df}{\int_{-\infty}^{\infty}p(f)\,df} \tag{2.24}$$

Making the definition $N^2 \equiv \overline{\Delta N^2}$, the root-mean-square noise becomes

$$N = \frac{\nu}{\pi\sqrt{2}}\sqrt{\theta\,(T)} \quad . \tag{2.25}$$

The general equation for the signal-to-noise ratio obtained by synchronous rectification can now be written. Taking the ratio of (2.4) to (2.25), we have

$$\frac{E}{N} = \frac{\pi\sqrt{2}}{\nu}\,\frac{\int_0^T e(t)e'(t)dt}{\sqrt{\theta\,(T)}} \quad . \tag{2.26}$$

This equation leads to the following conclusions. The signal-to-noise ratio obtained by the synchronous rectification system is dependent upon three functions:

1) the form and frequency of the target signal
2) the form of the reference signal
3) the power spectrum of the noise entering the correlator

A more detailed discussion of the effect of these three functions upon (2.26) will be given in Section IV.

In applying the analysis to a system having real components, deviations from the ideal transfer functions of the multiplier and integrator must be included in (2.26). This means that the Fourier series coefficients of e(t) and e'(t), and the power spectrum p(f) will take on a somewhat modified form.

III. THE TWO-DETECTOR CROSS-CORRELATION SYSTEM

A block diagram of this system is shown in Figure 2. The signal and noise waveforms included in the diagram again indicate the successive operations which improve the signal-to-noise ratio of the radiation detector. Radiation from a target passes through the chopper and falls on both of the detectors. The signals are then amplified and appear in the outputs of the pre-amplifiers as the waveforms indicated in Figure 2. The signals, containing both true signal and noise components, are then multiplied together and integrated.

The analysis of this system follows the same pattern as the preceding one. The two signals entering the multiplier will be written as

$$s_1(t) = e_1(t) + \Delta v_1(t), \tag{3.1}$$

and

$$s_2(t) = e_2(t) + \Delta v_2(t), \tag{3.2}$$

where $e_i(t)$ and $\Delta v_i(t)$ represent the true signal and noise components, respectively. The output of the integrator can then be written as

$$S(t) = \int_0^T s_1(t) s_2(t)\, dt \tag{3.3}$$

or

$$S(t) = \int_0^T [e_1(t)e_2(t) + e_1(t)\Delta v_2(t) + e_2(t)\Delta v_1(t) + \Delta v_1(t)\Delta v_2(t)]\, dt \quad . \tag{3.4}$$

The first term of (3.4) is the signal component in the output of the integrator,

$$E(t) = \int_0^T e_1(t)e_2(t)\,dt \quad . \tag{3.5}$$

The last three terms of (3.4) are the noise components in the output of the integrator.

The noise from these three terms can be written as

$$\Delta N(t) \equiv \Delta N_1(t) + \Delta N_2(t) + \Delta N_3(t) \quad , \tag{3.6}$$

where $\Delta N_1(t)$, $\Delta N_2(t)$, and $\Delta N_3(t)$ are defined by the equations

$$\Delta N_1(t) \equiv \int_0^T e_2(t)\Delta\nu_1(t)\,dt \quad , \tag{3.7}$$

$$\Delta N_2(t) \equiv \int_0^T e_1(t)\Delta\nu_2(t)\,dt \quad , \tag{3.8}$$

and

$$\Delta N_3(t) \equiv \int_0^T \Delta\nu_1(t)\Delta\nu_2(t)\,dt \quad . \tag{3.9}$$

Since the above three random noise variables are independent, it can easily be shown that

$$\overline{\Delta N^2} = \overline{\Delta N_1^2} + \overline{\Delta N_2^2} + \overline{\Delta N_3^2} \quad . \tag{3.10}$$

The first two terms in (3.10) have already been determined (see (2.3), (2.23), and (2.24)). The result is that

$$N_1^2 = \frac{\nu_1^2}{2\pi^2}\,\theta_1(T) \quad , \tag{3.11}$$

where

$$N_1^2 \equiv \overline{\Delta N_1^2} \quad , \quad \nu_1^2 \equiv \overline{\Delta\nu_1^2} \quad ,$$

and

$$\theta_1(T) \equiv \frac{\int_{-\infty}^{\infty} \left\{ \int_{-\infty}^{\infty} \psi_2(\tau) \cos 2\pi f\tau \left[\int_{-\infty}^{\infty} p_1(f) \cos 2\pi f\tau \, df \right] d\tau \right\} \frac{(1 - \cos 2\pi fT)}{f^2} df}{\int_{-\infty}^{\infty} p_1(f) \, df} \quad (3.12)$$

Similarly,

$$N_2^2 = \frac{\nu_2^2}{2\pi^2} \theta_2(T) \quad , \quad (3.13)$$

where

$$\theta_2(T) \equiv \frac{\int_{-\infty}^{\infty} \left\{ \int_{-\infty}^{\infty} \psi_1(\tau) \cos 2\pi f\tau \left[\int_{-\infty}^{\infty} p_2(f) \cos 2\pi f\tau \, df \right] d\tau \right\} \frac{(1 - \cos 2\pi fT)}{f^2} df}{\int_{-\infty}^{\infty} p_2(f) \, df} \quad (3.14)$$

The autocorrelation functions $\psi_1(\tau)$ and $\psi_2(\tau)$ are those corresponding to $e_1(t)$ and $e_2(t)$; $p_1(f)$ and $p_2(f)$ are the amplitude normalized power spectrums corresponding to $\Delta\nu_1(t)$ and $\Delta\nu_2(t)$.

The last term of (3.10) can be found by altering the form of (2.23) and (2.24). If the function $\psi'(\tau)$ is redefined as the autocorrelation function of $\Delta\nu_2(t)$, then $\psi'(\tau)$ can be written as

$$\psi'(\tau) \equiv \int_{-\infty}^{\infty} P_2(f) \cos 2\pi f\tau \, df \quad , \quad (3.15)$$

where $P_2(f)$ is the power spectrum of $\Delta\nu_2(t)$. It therefore follows that

$$N_3^2 = \frac{\nu_1^2 \nu_2^2}{2\pi^2} \theta_3(T) \quad , \quad (3.16)$$

where

$$\theta_3(T) \equiv \frac{\int_{-\infty}^{\infty} \left\{ \int_{-\infty}^{\infty} \left[\int_{-\infty}^{\infty} p_1(f) \cos 2\pi f\tau \, df \int_{-\infty}^{\infty} p_2(f) \cos 2\pi f\tau \, df \right] \cos 2\pi f\tau \, d\tau \right\} \frac{(1 - \cos 2\pi fT)}{f^2} df}{\int_{-\infty}^{\infty} p_1(f) \, df \int_{-\infty}^{\infty} p_2(f) \, df} \quad (3.17)$$

Using (3.11), (3.13), and (3.16) the root-mean-square noise in the output of the integration can be obtained:

$$N = \frac{\nu_1 \nu_2}{\pi\sqrt{2}} \left\{ \theta_3(T) + \frac{1}{\nu_1^2}\, \theta_2(T) + \frac{1}{\nu_2^2}\, \theta_1(T) \right\}^{1/2} \quad . \tag{3.18}$$

Taking the ratio of (3.5) to (3.18), there follows that

$$\frac{E}{N} = \frac{\pi\sqrt{2}}{\nu_1 \nu_2} \frac{\int_0^T e_1(t)\, e_2(t)\, dt}{\sqrt{\theta(T)}} \quad , \tag{3.19}$$

where

$$\theta(T) \equiv \theta_3(T) + \frac{1}{\nu_1^2}\, \theta_2(T) + \frac{1}{\nu_2^2}\, \theta_1(T) \quad . \tag{3.20}$$

This equation should be compared with (2.26). The signal-to-noise ratio obtained by cross-correlation is dependent upon the form and frequency of the target signals and the power spectrums of the noise entering the correlator. In the following section a detailed expression for the ratio E/N will be discussed. As in the previous system, deviations from the ideal transfer functions of the multiplier and integrator must be included in (3.19), if the analysis is to be interpreted in terms of real system components.

IV. IMPROVEMENTS IN SIGNAL-TO-NOISE RATIO

The results of Sections II and III provide a general description of the improvement in the signal-to-noise ratio which can be obtained with each system. A more detailed description requires that assumptions be made concerning the form and frequency of the target and reference signals as well as the form of the power spectrum of the noise entering the correlator. In the analysis which follows the synchronous rectification system will be treated first.

The true signal component of (2.1) we shall assume to be a sine wave of frequency f_0 and amplitude ε,

$$e(t) = \varepsilon \sin 2\pi f_0 t \quad . \tag{4.1}$$

The reference signal will be taken as

$$e'(t) = \varepsilon' \sin 2\pi f_0 t \quad . \tag{4.2}$$

This equation permits the determination of the autocorrelation function $\psi'(\tau)$ appearing in (2.24). From (2.14) it follows that

$$\psi'(\tau) = \frac{\varepsilon'^2}{2} \cos 2\pi f_0 \tau \quad . \tag{4.3}$$

Furthermore, the integral appearing in (2.26) can now be evaluated.

$$E = \int_0^T e(t)e'(t)\,dt = \frac{\varepsilon\varepsilon'}{2}\left(1 - \frac{\sin 4\pi f_0 T}{4\pi f_0 T}\right) T \quad . \tag{4.4}$$

For $f_0 T \geq 10$ ($< 1\%$ error),

$$E = \frac{\varepsilon \varepsilon'}{2} T \quad . \tag{4.5}$$

The remaining function needed to evaluate (2.26) is the power spectrum of the noise entering the correlator. Some difficulty is encountered in selecting a power spectrum which is sufficiently general in form and yet reasonable to handle mathematically. Perhaps the most satisfactory one has the following form:

$$p(f) = \begin{cases} 1 \ , & \text{for } f_1 \leq f \leq f_2 \ , \ -f_2 \leq f \leq -f_1 \\ 0 \ , & \text{for } -f_1 < f < f_1 \ , \ f > f_2 \ , \ f < -f_2 \end{cases} \ , \tag{4.6}$$

where f_1 and f_2 determine the bandwidth Δf of the noise. A diagram of (4.6) is given in Figure 3.

On the basis of (4.3) and (4.6), the function $\theta(T)$ of (2.26) may be evaluated. The result is that

$$\theta(T) = \frac{\varepsilon'^2}{2(f_2 - f_1)} \left\{ \frac{1}{2(f_0 + f_1)} - \frac{1}{2(f_0 + f_2)} - \frac{1}{2(f_0 - f_1)} - \frac{1}{2(f_2 - f_0)} \right. \tag{4.7}$$

$$+ \frac{\cos 2\pi T(f_0 - f_1)}{2(f_0 - f_1)} + \frac{\cos 2\pi T(f_2 - f_0)}{2(f_2 - f_0)} + \frac{\cos 2\pi T(f_0 + f_2)}{2(f_0 + f_2)}$$

$$- \frac{\cos 2\pi T(f_0 + f_1)}{2(f_0 + f_1)} + \pi T \, \mathrm{Si}\, 2\pi T(f_0 + f_2) - \pi T \, \mathrm{Si}\, 2\pi T(f_0 + f_1)$$

$$\left. + \pi T \, \mathrm{Si}\, 2\pi T(f_0 - f_1) + \pi T \, \mathrm{Si}\, 2\pi T(f_2 - f_0) \right\} \ ,$$

where the function Si(x) is defined as

$$\mathrm{Si}(x) \equiv \int_0^x \frac{\sin u}{u} \, du \quad . \tag{4.8}$$

The above function converges very rapidly to $\pi/2$ as $x \to \infty$; for $x \geq 10$ $Si(x) \approx \pi/2$ (within 6 %). An exhaustive treatment of the function can be found in Ref. 19, pp. 1 - 9.

The Equation (2.26) can now be written explicitly:

$$\frac{E}{N} = \frac{\pi}{\sqrt{2}} \left(\frac{\varepsilon}{\nu}\right) \varepsilon' \left(1 - \frac{\sin 4\pi f_0 T}{4\pi f_0 T}\right) \frac{T}{\sqrt{\theta(T)}} \quad , \qquad (4.9)$$

where $\theta(T)$ is given by (4.7). The signal-to-noise ratio obtained by synchronous rectification depends upon a complex function of the chopping frequency, bandwidth, and integration time.

A close study of (4.9) reveals that a number of important trends can be determined. E/N approaches zero as T^2 for very small T, and varies as the square root of the integration time for very large T. Between the limiting values of T oscillations occur in a somewhat complex manner.

The effect of the chopping frequency f_0 and bandwidth Δf upon the improvement in the signal-to-noise ratio is also significant. The most satisfactory way to determine this effect is to discuss the form of the power spectrum of the multiplied noise (see (2.19)). The reason for this approach is that the integrator network following the multiplier operates as a low-pass filter. The transfer function of an integrator network integrating over a period of time T can be shown to have the following form:

$$W_i(f) = \frac{1}{2\pi f} \left\{\sin 2\pi fT + j(\cos 2\pi fT - 1)\right\} .$$

In terms of this equation (2.17) becomes

$$N^2 = \int_{-\infty}^{\infty} \Phi(f) \left| W_i(f) \right|^2 df \quad . \qquad (4.10)$$

The function $\left| W_i(f) \right|^2$ is shown in graphical form in Figure 4.

It is apparent from the above two equations (and from (2.17) that the mean-square noise in the output of the integrator is much smaller for power spectrums having components predominantly at high frequency. We now proceed to a discussion of the power spectrum of the multiplied noise.

When (2.19) is evaluated three cases are observed in the result: (a) $f_0 - f_1 \leq f_2 - f_0 \leq f_0 + f_1$; (b) $f_2 - f_0 \leq f_0 - f_1 \leq f_0 + f_1$; and (c) $f_0 - f_1 \leq f_0 + f_1 \leq f_2 - f_0$. The power spectrums corresponding to these cases are shown in Figure 5 a, b, and c. These graphs show that low frequency components appear in the power spectrum of the multiplied noise that did not appear at all in the power spectrum of the cell noise (see (4.6)). Furthermore, no manipulation of the bandwidth or signal frequency f_0 can eliminate these low frequencies. The most that can be done is to minimize the contribution to the integral in (4.10) due to the low frequencies, and push as much of the power spectrum as possible into the high frequency range. To accomplish this f_0 should be set equal to f_2; the chopping frequency f_0 should be as high as possible, since (from Figure 5 a, b) the high frequency components in the power spectrum are dependent upon its magnitude. The results of prescribing these conditions is that the value of the integral in (4.10) will be minimized.

Having discussed qualitatively the effects of integration time and power spectrum upon the root mean-square correlated noise, (4.9) may now be represented graphically. However, let us first define a quantity Q(T) as follows:

$$Q(T) = \frac{(E/N)}{(\varepsilon/\nu)} \quad . \tag{4.11}$$

Q(T) represents the improvement in signal-to-noise ratio obtained for a given integration time and noise bandwidth. Written in terms of Q(T), (4.9) becomes

$$Q(T) = \frac{\pi}{\sqrt{2}} \varepsilon' \left(1 - \frac{\sin 4\pi f_0 T}{4\pi f_0 T}\right) \frac{T}{\sqrt{\theta(T)}} \quad . \tag{4.12}$$

Figure 6 shows a graph of (4.12) for $Q(T) > 1$ and for various values of the parameter Δf. The signal frequency f_0 has been set equal to the high frequency limit f_2 of the band pass. The function $Q(T)$, as shown in the graph, increases as the square root of the time-bandwidth product. It should be pointed out that the dependence of $Q(T)$ upon the square root of the bandwidth Δf is somewhat misleading, since the initial signal-to-noise ratio is inversely proportional to the square root of the bandwidth.

A graph of an additional function $Q^*(T)$ is shown in Figure 7. This function represents the improvement in signal-to-noise ratio for noise of unit bandwidth ($f_2 - f_1 = 1$). The band has been moved over the frequency spectrum by assigning values to the center frequency $f_c \equiv (f_1 + f_2)/2$. We may conclude from the figure that for improvements of magnitude $Q(T) > 1$, the system operates nearly independently of where the bandwidth Δf is located in the frequency spectrum. In other words, the advantage obtained with high chopping frequencies is negligibly small.

Proceeding to the two-detector cross-correlation system, we shall make the same assumptions with regard to the target signals and the power spectrums of the cell noise as in the previous system. The true signal components in (3.1) and (3.2) will be written as

$$e_1(t) = \varepsilon_1 \sin 2\pi f_0 t \tag{4.13}$$

$$e_2(t) = \varepsilon_2 \sin 2\pi f_0 t \quad . \tag{4.14}$$

The autocorrelation functions appearing in $\theta_1(T)$ and $\theta_2(T)$ (see (3.12) and (3.14) can be obtained from (2.14):

$$\psi_1(\tau) = \frac{\varepsilon_1^2}{2} \cos 2\pi f_0 \tau \quad , \tag{4.15}$$

and

$$\psi_2(\tau) = \frac{\varepsilon_2^2}{2} \cos 2\pi f_0 \tau \quad . \tag{4.16}$$

Using the above two equations, (4.13) and (4.14), the integral in (3.19) can be evaluated to give

$$\int_0^T e_1(t)e_2(t)\,dt = \frac{\varepsilon_1\varepsilon_2}{2}\left(1 - \frac{\sin 4\pi f_0 T}{4\pi f_0 T}\right)T \quad . \tag{4.17}$$

For $f_0 T \geq 10$ (< one per cent error),

$$\int_0^T e_1(t)e_2(t)\,dt = \frac{\varepsilon_1\varepsilon_2}{2}\,T \quad . \tag{4.18}$$

The power spectrums of the cell noise, $p_1(f)$ and $p_2(f)$, are assumed to be identical, and of the same form as (4.6); that is,

$$p_1(f) = p_2(f) = \begin{cases} 1 & , \text{ for } f_1 \leq f \leq f_2 \,, -f_2 \leq f \leq -f_1 \\ 0 & , \text{ for } -f_1 < f < f_1 \,, f > f_2 \,, f < -f_2 \end{cases} \quad . \tag{4.19}$$

With the above assumptions the equation (3.19) can be carried out explicitly. The result is

$$\frac{E}{N} = \frac{\pi}{\sqrt{2}}\left(1 - \frac{\sin 4\pi f_0 T}{4\pi f_0 T}\right)\frac{\varepsilon_1}{\nu_1}\,\frac{\varepsilon_2}{\nu_2}\,\frac{T}{\sqrt{\theta(T)}} \quad , \tag{4.20}$$

where

$$\theta(T) = \theta_3(T) + \frac{1}{\nu_1^{\,2}}\,\theta_2(T) + \frac{1}{\nu_2^{\,2}}\,\theta_1(T) \quad , \tag{4.21}$$

and

$$\begin{aligned}\theta_3(T) = \frac{1}{2(f_2 - f_1)^2}\Big\{ & -2 - 2\ln\gamma - \ln 4f_1 f_2 + 2\ln\frac{(f_2 + f_1)}{(f_2 - f_1)} - 2\ln 2\pi T \\ & + \cos 4\pi f_2 T + \cos 4\pi f_1 T + 4\sin 2\pi f_2 T \sin 2\pi f_1 T + \mathrm{Ci}(4\pi f_2 T) \\ & + \mathrm{Ci}(4\pi f_1 T) - 2\mathrm{Ci}\,2\pi(f_2 + f_1)T + 2\mathrm{Ci}\,2\pi(f_2 - f_1)T + 4\pi f_2 T\,\mathrm{Si}\,4\pi f_2 T \\ & + 4\pi f_1 T\,\mathrm{Si}\,4\pi f_1 T - 4\pi f_1 T\,\mathrm{Si}\,2\pi(f_2 - f_1)T - 4\pi f_1 T\,\mathrm{Si}\,2\pi(f_2 + f_1)T \\ & - 4\pi f_2 T\,\mathrm{Si}\,2\pi(f_2 + f_1)T + 4\pi f_2 T\,\mathrm{Si}\,2\pi(f_2 - f_1)T\Big\}\end{aligned} \tag{4.22}$$

$$\theta_2(T) = \frac{\varepsilon_1^2}{2(f_2 - f_1)}\left\{\frac{1}{2(f_0 + f_1)} - \frac{1}{2(f_0 + f_2)} - \frac{1}{2(f_0 - f_1)} - \frac{1}{2(f_2 - f_0)}\right.$$

$$+ \frac{\cos 2\pi T(f_0 - f_1)}{2(f_0 - f_1)} + \frac{\cos 2\pi T(f_2 - f_0)}{2(f_2 - f_0)} + \frac{\cos 2\pi T(f_0 + f_2)}{2(f_0 + f_2)}$$

$$- \frac{\cos 2\pi T(f_0 + f_1)}{2(f_0 + f_1)} + \pi T \,\mathrm{Si}\, 2\pi T(f_0 + f_2) - \pi T \,\mathrm{Si}\, 2\pi T(f_0 + f_1) \qquad (4.23)$$

$$\left. + \pi T \,\mathrm{Si}\, 2\pi T(f_0 - f_1) + \pi T \,\mathrm{Si}\, 2\pi T(f_2 - f_0)\right\} \quad .$$

$$\theta_1(T) = \frac{\varepsilon_2^2}{2(f_2 - f_1)} \quad \frac{1}{2(f_0 + f_1)} - \frac{1}{2(f_0 + f_2)} - \frac{1}{2(f_0 - f_1)} - \frac{1}{2(f_2 - f_0)}$$

$$+ \frac{\cos 2\pi T(f_0 - f_1)}{2(f_0 - f_1)} + \frac{\cos 2\pi T(f_2 - f_0)}{2(f_2 - f_0)} + \frac{\cos 2\pi T(f_0 + f_2)}{2(f_0 + f_2)} \qquad (4.24)$$

$$- \frac{\cos 2\pi T(f_0 + f_1)}{2(f_0 + f_1)} + \pi T \,\mathrm{Si}\, 2\pi T(f_0 + f_2) - \pi T \,\mathrm{Si}\, 2\pi T(f_0 + f_1)$$

$$\left. + \pi T \,\mathrm{Si}\, 2\pi T(f_0 - f_1) + \pi T \,\mathrm{Si}\, 2\pi T(f_2 - f_0)\right\} \quad .$$

The constant γ is equal to 1.781. The function Ci(x) is defined as

$$\mathrm{Ci}(x) \equiv -\int_x^\infty \frac{\cos u}{u}\, du \qquad (4.25)$$

As x becomes large the function Ci(x) converges rapidly to zero as $(\sin x)/x$; for $x \geq 10$, $\mathrm{Ci}(x) \leq 0.1$. The function is treated fully in Reference 19, pp. 1 - 9.

As in the previous system the rate at which E/N increases depends upon a complex function of the chopping frequency, bandwidth and integration time. However, some qualitative remarks may be made. For very small values of T the signal-to-noise ratio goes

to zero as T^2; for large values of T, it increases as the square root of T. Between these limiting values no general characteristics can be obtained since the function behaves complexly.

Let us consider the effect of the chopping frequency and the power spectrums of the cell noise upon (4.20). The three components of the noise in the output of the integrator stage are given in Equations (3.6) through (3.9). The first two components in (3.6) are cross terms involving the target and cell noise signals. The power spectrums of each of these terms are nearly identical to those in Figure 5 a, b, and c; the only changes are in the substitution of ε_1 or ε_2 for ε' and $P_{1\,max}$ or $P_{2\,max}$ for P_{max}. These power spectrums are shown in Figures 8 and 9. The third component of (3.6) has a power spectrum as shown in Figure 10. The power spectrum of $\Delta N(t)$ is, of course, the sum of the three component spectrums.

From the above three figures some conclusions can be reached for optimum correlator efficiency: 1) the chopping frequency should be kept very near the upper band-pass limit; that is, $f_0 \approx f_2$; and 2) the chopping frequency should be as high as possible. These conclusions follow from the fact that the integrator stage operates as a low-pass filter (see (2.17)).

If the signal-to-noise ratios ε_1/ν_1 and ε_2/ν_2 are assumed to be equal (defined as ε/ν), then (4.20) may be written in terms of the function Q(T). The equation becomes

$$Q(T) = \frac{\pi}{\sqrt{2}} \left(1 - \frac{\sin 4\pi f_0 T}{4\pi f_0 T}\right) \frac{\varepsilon}{\nu} \frac{T}{\sqrt{\theta(T)}} , \qquad (4.26)$$

where $\theta(T)$ is given by (4.21) through 4.24). The only significant difference between this equation and (4.12) is that an additional factor ε/ν has appeared: Q(T) is now dependent upon the original signal-to-noise ratio. If the ratio ε/ν is set equal to unity, then a graph of (4.26) may be made similar to that in Figure 6. The graph is shown in Figure 11. The signal frequency f_0 has again been given the same value as f_2. As in Figure 6 the function Q(T) increases as the square root of the time-bandwidth product, for $Q(T) > 1$. However, it should

be remembered that the original signal-to-noise ratio ε/ν is inversely proportional to the square root of the bandwidth.

A graph of $Q^*(T)$ for the two-detector cross-correlation system is shown in Figure 12. The signal-to-noise ratio ε/ν has been set equal to unity; and f_0, to f_2. As in synchronous rectification the improvement in signal-to-noise ratio for $Q(T) > 1$ is nearly independent of where the bandwidth is located in the frequency spectrum. That is, no significant advantage is gained by going to high chopping frequencies.

Several conclusions can be obtained by comparing Figures 6 and 11. The curves in Figure 11 show a constant displacement downward of a factor of 2.45 from the curves in Figure 6. The cause of these lower $Q(T)$ values are the additional two terms in the noise output of the correlator (see (3.6)). A second conclusion relates to the dependence of $Q(T)$ in two-detector cross-correlation upon the original signal-to-noise ratio. If another value for ε/ν were selected for Figure 11 th curves would be displaced. The trends in the displacement will be the following: 1) for $\varepsilon/\nu \ll 1$, $Q(T)$ is proportional to the first power of ε/ν; and 2) for $\varepsilon/\nu \gg 1$, $Q(T)$ is independent of the original signal-to-noise ratio. Thus synchronous rectification and two-detector cross-correlation are nearly equivalent for $\varepsilon/\nu \gg 1$. For $\varepsilon/\nu \ll 1$, the improvement in signal-to-noise ratio in cross-correlation is less than that in synchronous rectification by a factor of $2/(\varepsilon/\nu)$.

V. RETICLE AND SCANNING SYSTEMS

An important topic to be considered is the application of correlation techniques to reticle and scanning systems performing search and tracking operations. The primary function of these systems is to indicate the presence and position of the target within a specified field of view. This section discusses the transfer of positional information by the synchronous rectification and two-detector cross-correlation systems.

In reticle systems the position of the target is obtained from information inherent in the signal waveform. The sources of information are the phase, frequency, and amplitude of the signal. Various combinations of these sources are used to locate the target in the field of view. For instance, in the Sidewinder system the phase and amplitude of the signal provide the angular and radial information necessary for locating the target. When applying correlation techniques to reticle systems, the immediate problem is how to transfer positional information in the target signal and yet retain a relatively high information rate. Since positional information depends upon the shape of the signal waveform it necessarily follows that the correlation time must be short compared with the period of the signal. Otherwise, the original shape of the target signal is lost. The difficulty in obtaining significant improvements in signal-to-noise ratio for short correlation times ($\sim 10^{-2}$ sec) can be easily seen from Figures 6 and 11. Only for systems having wide noise bandwidths ($\gtrsim 10$ kc) is this possible; for narrower bandwidths, the improvements are very small. Improvements in signal-to-noise ratio are accompanied by a reduction in information rate. We may, therefore, make the following conclusion: in reticle

systems requiring high rates of position information, it would appear that correlation techniques will find no application, unless the condition $(\Delta f/f_0) \geq 10^3$ is met.

The scanning systems referred to are those using the scanning spot and multiple-scanning spot. The single spot obtains target position information by systematically scanning and sampling small elements within the total field of view. The small element representing the instantaneous field of view localizes the target in the scanning pattern. The multiple-scanning spot is a linear array of single spots performing a one-dimensional scan to cover the field of view. Several detectors are used in this system, each one covering a portion of the scanning pattern. In both of these methods, the required improvement in signal-to-noise ratio and noise bandwidth of the system will determine the minimum dwell time of the scanning operation. The dwell time is to be equated with the correlation time. The design of the scanning system will then consist of a compromise between the parameters of information rate, total field of view, and instantaneous field of view. If low rates of target position information are acceptable in the design of a scanning system, then application of correlation techniques should give significant improvement in the signal-to-noise ratio of the system.

The multiple scanning-spot method implies the use of more than one correlator in the scanning operation. This, in turn, raises the question of the size and weight of correlation systems. Early in 1960 work was begun on the production of a miniaturized correlator. The result was a correlator composed of a Hall-effect multiplier and an RC filter acting as the integrator. A photograph of the system is shown in Figure 13. More than just the correlator is shown in the photograph. The multiplier unit is located in the upper right-hand corner; the integrator unit is in the lower right-hand corner. The elements on the left side of the photograph are transitor amplifiers which drive the Hall-effect multiplier. A free-running multivibrator circuit coupled with a relay was used to control the integration time over a period of about 0.25 seconds to 5 seconds. The scale at the

bottom of the picture is in inches; the third dimension of the correlator is about two inches. Figure 14 shows a circuit diagram of the correlator components and transistor amplifiers. The frequency response of the multiplier is limited only by the characteristics of the coil, since the response of the Hall element itself extends well into the megacycle region. In summary we may conclude that correlators may be obtained which occupy a volume of four or five cubic inches and have a weight of a few ounces.

One additional application of correlation techniques should be mentioned. A correlation system may be used to replace the cooling system of certain detectors; that is, detectors whose signal-producing mechanism is not impaired at room temperature. However, it should be emphasized that the use of a correlator will considerably increase the response time of the detection system. Recently, a successful experiment of this type was carried out with photoconductive InSb cells operating at room temperature. With a noise bandwidth of one kilocycle and an initial signal-to-noise ratio of unity, an order of magnitude improvement in cell detectivity may be obtained in a correlation time of 0.20 seconds. An order of magnitude improvement in detectivity is equivalent to cooling the cell to dry-ice temperature (195°K). See Reference 20, p. 1467 f.

VI. THE EXPERIMENTAL STUDY

Many correlators have been constructed for the purpose of utilizing the properties of the correlation function. Among these may be distinguished two classes: the sampling correlator and the continuous correlator. The first class of correlators operates by sampling each time dependent function entering the multiplier stage over a given period of time; then the corresponding samples are multiplied and added together. Correlators of this type include those of Cowley[21] (1949), Singleton[22](1950), and Cheatham[23](1951). The second class of correlators performs a continuous operation of multiplying the two functions together and then integrating (averaging) the result. Stevens[24](1950), Fano[25](1950), Faran and Hills[26](1952), and Johnson[27](1952) have described correlators of this type. The correlator developed at NSL belongs to the second class.

The two-detector cross-correlation system, incorporating the NSL correlator is shown in schematic form in Figure 15 and in pictorial form in Figure 16. The radiation source is a Sylvania glow modulator tube, Type R1131C, modulated by a sinusoidal waveform. The modulated radiation source is a convenient component for the system since it eliminates the necessity of a chopper and provides a target signal of known form. The two PbS cells are mounted adjacently at the end of a brass tube. Since ac pickup is quite large in a high-gain network, the radiation source and detector assembly components are placed within a metal container (Figure 17). The preamplifier units following the PbS cells are Tektronix, Type 122, low-noise amplifiers. Bandwidth settings include the following: low frequency cutoffs (3 db), 0.2, 0.8, 8, and 80 cps; high frequency cutoffs (3 db), 50, 250, 1000, 10000, and

40000 cps. Gain settings are approximately 100 and 1000. The multiplier stage of the correlator is a Philbrick, Model HM, combined multiplier/operational fivefold. This hybrid component is designed for special purpose applications in analogue computing operations, and consists of a multiplier unit and five K2-W operational amplifier units. The multiplier has a dynamic range of − 50 to + 50 volts dc, a maximum d-c error below one per cent of full scale, and a band pass of dc to 15 kilocycles. The integrator stage of the correlator uses one of the operational amplifier units, the remaining four being used as additional amplification stages beyond that of the preamplifiers.

Oscilloscope pictures have been taken which illustrate in a graphical manner the operation of the correlator. Figure 18a shows a picture of the waveforms entering the two input channels of the correlator. The waveforms consist of a noise component alone: no radiation (target) signal is present. Figure 18b shows the output of the correlator, the integrator unit integrating successively over a period of 0.4 sec.; that is, the integrator is shorted out every 0.4 sec. The square divisions along the abscissa are calibrated to 0.2 sec per division. The zero line is located just below the central line of the picture. Figure 19a and b shows the change in the output of the correlator when a small sinusoidal target signal is introduced into the two input channels. Despite the small signal-to-noise ratio, the output of the correlator (Figure 19b) shows in a remarkable way the presence of the signal component. The successive integrations are again carried out over a period of about 0.4 sec. The scale along the abscissa is 0.2 sec per division, and the zero line is located three square divisions from the bottom of the picture.

To confirm the theoretical analysis of the two-detector cross-correlation system, (3.19) must be evaluated. Since the target signal is sinusoidal, the only functions needed to evaluate (3.19) are the amplitude-normalized power spectrums of the noise entering the correlator. These are obtained by means of a Brüel and Kjaer AF spectrometer (see Figure 20a, b). Since $p_1(f)$ and $p_2(f)$ are not analytic, a computer program was set up to evaluate (3.12), (3.14), and (3.17). The program

was carried out on an IBM 704 computer at the M. I. T. Computation Center. The results are shown in Figures 21 and 22 as the solid lines. The signal frequency f_0 was 500 cps, the initial signal-to-noise ratios were 1.0 and 0.50, and the equivalent bandwidths of the noise, Δf_1^* and Δf_2^*, were 1.16 kc and 1.04 kc. The signal-to-noise ratios entering both channels of the correlator were equal.

From the experimental study, data points were obtained giving the improvement in the signal-to-noise ratio Q(T) in terms of the noise bandwidths, integration time, and initial signal-to-noise ratio. Two such series of data points are given in Figures 21 and 22.

The low initial signal-to-noise ratios of 1.00 and 0.50 were produced by noting the linearity of the glow modulator, detector, and preamplifier system. The voltage across the glow modulator tube is proportional to the preamplifier output voltage over a wide range of voltages. In addition to the initial signal-to-noise ratio ε/ν, the two quantities required to determine Q(T) are E(T) and N(T). A statistical sampling procedure was followed in measuring these quantities, the samples being recorded on a Honeywell Visicorder. From the tapes, average and root-mean-square values of E(T) and N(T), respectively, were obtained.

We proceed now to an error analysis of the experimental data points determining the function Q(T). Since Q(T) is defined by the equation

$$Q(T) \equiv \frac{(E/N)}{(\varepsilon/\nu)} \tag{6.1}$$

it follows that

$$\frac{\Delta Q(T)}{Q(T)} \approx \frac{\Delta E}{E} + \frac{\Delta \nu}{\nu} - \frac{\Delta N}{N} - \frac{\Delta \varepsilon}{\varepsilon} \quad . \tag{6.2}$$

The root-mean-square fractional error in Q(T) is therefore

$$\Delta \equiv \left[\frac{\overline{\Delta Q^2(T)}}{Q^2(T)}\right]^{1/2} = \left[\frac{\overline{\Delta E^2}}{E^2} + \frac{\overline{\Delta \nu^2}}{\nu^2} + \frac{\overline{\Delta N^2}}{N^2} + \frac{\overline{\Delta \varepsilon^2}}{\varepsilon^2}\right]^{1/2} \quad . \tag{6.3}$$

The terms on the right-hand side of (6.3) can be obtained by estimating the accuracy of the measurement of each term. The fractional error in measuring ε and ν was about 0.02 and 0.05, respectively. The number of samples taken in measuring E(T) and N(T) was 25. In the case of E(T) the error varies as a function of the correlation time, and has a range of values from about 0.05 to about 0.03. The fractional error in N(T) is approximately equal to the reciprocal of the square root of the number of samples taken. With a sampling number of 25, the rms error is about 0.20. Thus the principle contribution to the error in Q(T) is due to the function N(T). Using the above estimates (6.3) can be evaluated to give

$$\Delta \approx 21 \text{ per cent} \tag{6.4}$$

If the scatter of the data points around the computed value of Q(T) is assumed to follow a Gaussian probability distribution, then 68 per cent of the data points (or 2 out of 3) should lie within one standard deviation. Figures 21 and 22 agree with this assumption.

We may conclude, therefore, that within the limits of experimental error, substantial agreement was obtained between the theoretical analysis and the experimental study.

VII. SUMMARY

In this report we have reviewed the possibility of applying correlation techniques to improve the signal-to-noise ratio of infrared detection systems. General expressions have been derived which describe the operation of two correlation systems that can be used for this purpose. A detailed analysis for systems having band-limited white noise and sinusoidal target signals has also been presented. The most promising applications of these techniques appear to be with scanning systems and mosaics where high information rates are not required. An experimental study of the two-detector cross-correlation system has confirmed the theoretical analysis of this system.

REFERENCES

1. Wiener, N. Acta Mathematica (Stockholm), 55 pp. 117-258 (1930).
2. Wood, Frank Bradshaw. (ed.) The Present and Future of the Telescope of Moderate Size. Philadelphia: University of Pennsylvania Press, 1958.
3. Barlow, J.S. and Brown, R.M. An Analogue Correlator System for Brain Potentials. RLE, M.I.T. Technical Report 300, July, 1955.
4. Bivans, E. W. and Chatterton, E.J. Modulation Characteristics of Turbulent Infrared Sources. M.I.T. Lincoln Laboratory Group Report 52-5, February, 1959. (Secret)
5. Lee, Y. W. and Wiesner, J.B. Electronics, 23, pp.86-92(1950).
6. Lee, Y. W., Cheatham, T.P., and Wiesner, J.B. Proc. of IRE, 38, pp. 1165-1171 (1950).
7. Fano, R.M. Signal-to-Noise Ratio in Correlation Detectors. RLE, M.I.T. Technical Report 186, February, 1951.
8. Davenport, W.B. Jr. Correlator Errors Due to Finite Observation Intervals. RLE, M.I.T. Technical Report 191. March, 1951.
9. Dicke, R.H. Review of Scientific Instruments, 17, pp. 268-275 (1946).
10. Goldstein, S.J. Proc. IRE, 43, p. 1663 ff. (1955).
11. Jacobson, M.J. Analysis of a Multiple Receiver Correlation System. Troy, New York: Rensselaer Polytechnic Institute, RPI Math Report No. 8. May 13, 1957.
12-14. Statistical Theory of Communication. Research Laboratory of Electronics, M.I.T. January, April, and July (1950).
15. North, D.O. Analysis of the Factors which Determine Signal-to-Noise Discrimination in Radar. RCA Laboratories Report PTR-6C. June, 1943.
16. Van Vleck, J. and Middleton, D. Journal of Applied Physics, 17, pp. 940-971 (1946).

17. Zadeh, L.A. and Raggazzini, J.R. Proc. IRE, 40, pp. 1223-1231 (1952).

18. Davenport, W.B. Jr. and Root, W.L. Random Signals and Noise. New York: McGraw-Hill Book Company, Inc., 1958.

19. Jahnke, E. and Emde, F. Tables of Functions. New York: Dover Publications, 1945.

20. Rieke, F.F., DeVaux, L.H., and Tuzzolino, A.J. Proc. IRE, 47, pp. 1475-1478. (1959).

21. Cowley, P.E.A. A Short Time Correlator for Speech Waves. Master Thesis, E.E. Department, M.I.T., Cambridge, Mass. 1949.

22. Singleton, H.E. A Digital Electronic Correlator. RLE, M.I.T. Technical Report 152, February, 1950.

23. Cheatham, T.P. An Electronic Correlator. RLE, M.I.T. Technical Report 122, March, 1951.

24. Stevens, K.N. Journal of the Acoustical Society of America, 23, pp. 769-771(1950).

25. Fano, R.M. Journal of the Acoustical Society of America, 22, pp. 546-550 (1950).

26. Faran, J.J.Jr. and Hills, R.Jr. Correlators for Signal Reception. Acoustical Research Laboratory, Harvard University. TM 27 (1952).

27. Johnson, R.A. An Analog Computer for Correlation Functions in Communication Systems. Harvard University, Cruft Laboratory Technical Report 144 (1952).

28. Freeman, J.J. Principles of Noise. New York: John Wiley and Sons, Inc. 1958.

ILLUSTRATIONS

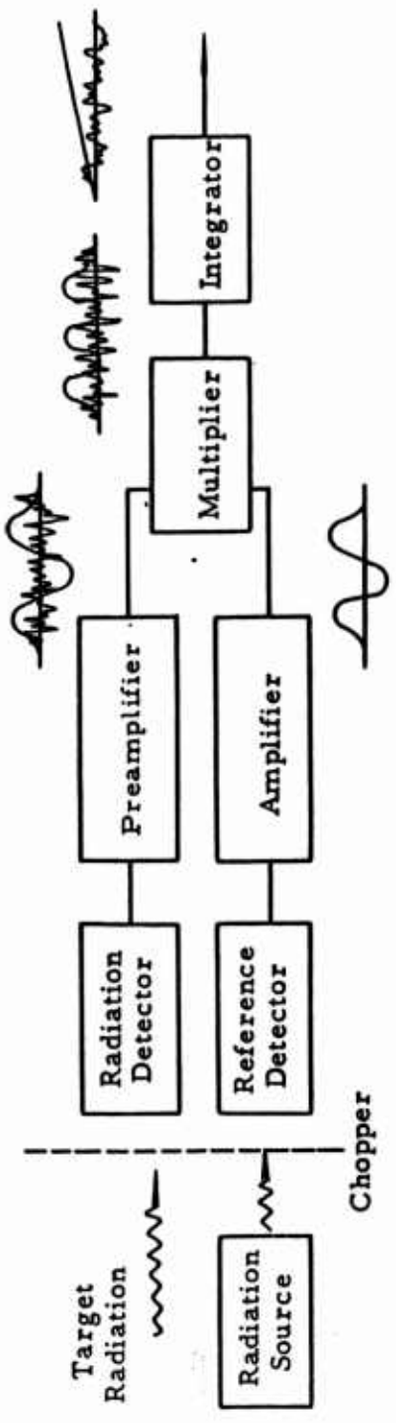

Figure 1. Block Diagram for Operation of the Synchronous Rectification System

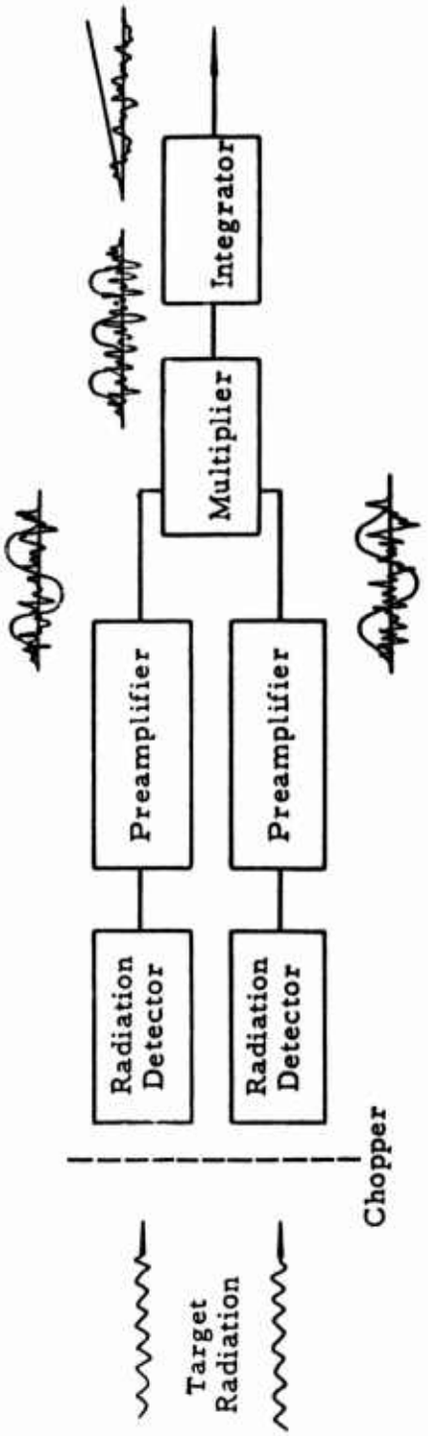

Figure 2. Block Diagram for Operation of the Two-Detector Cross-Correlation System

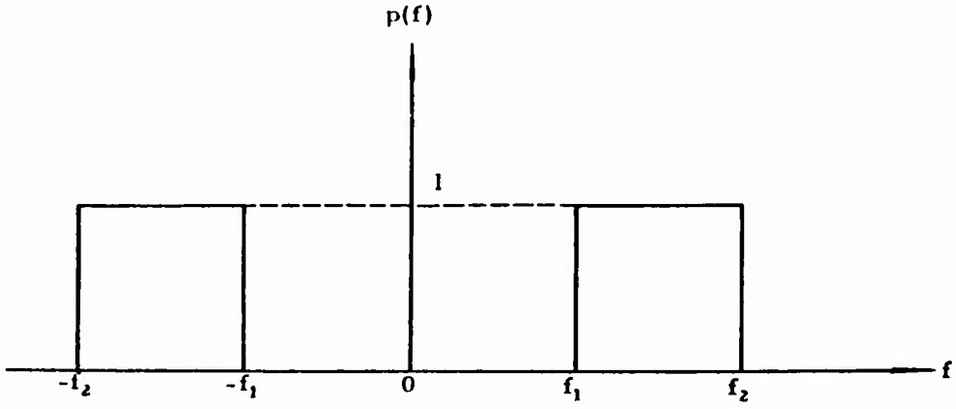

Figure 3. Amplitude-Normalized Power Spectrum of $\Delta\nu(t)$

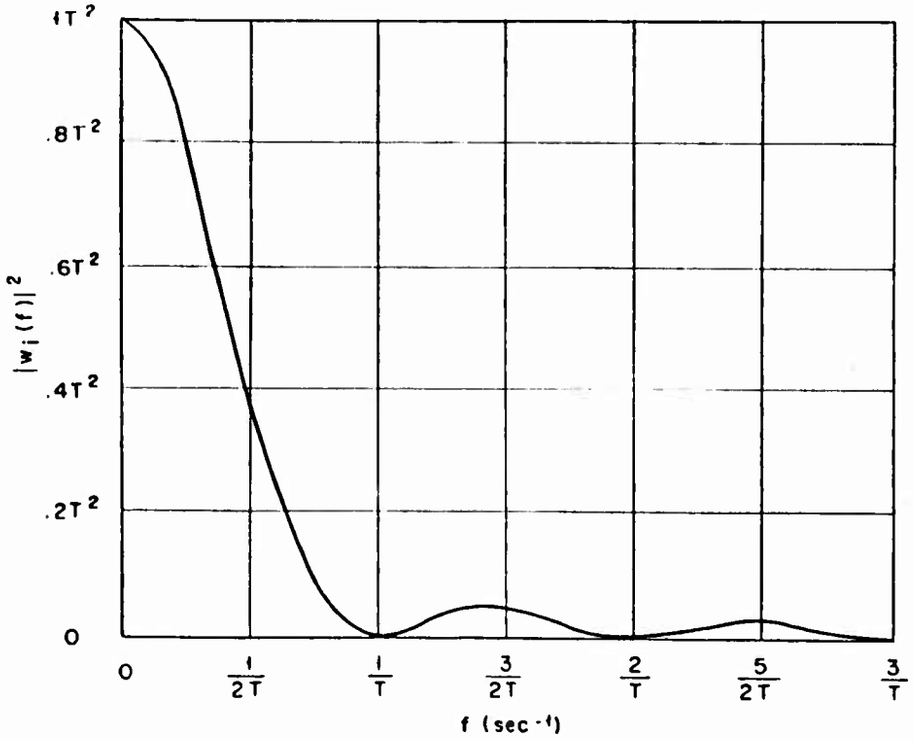

Figure 4. Transfer Function of an Integrator Network

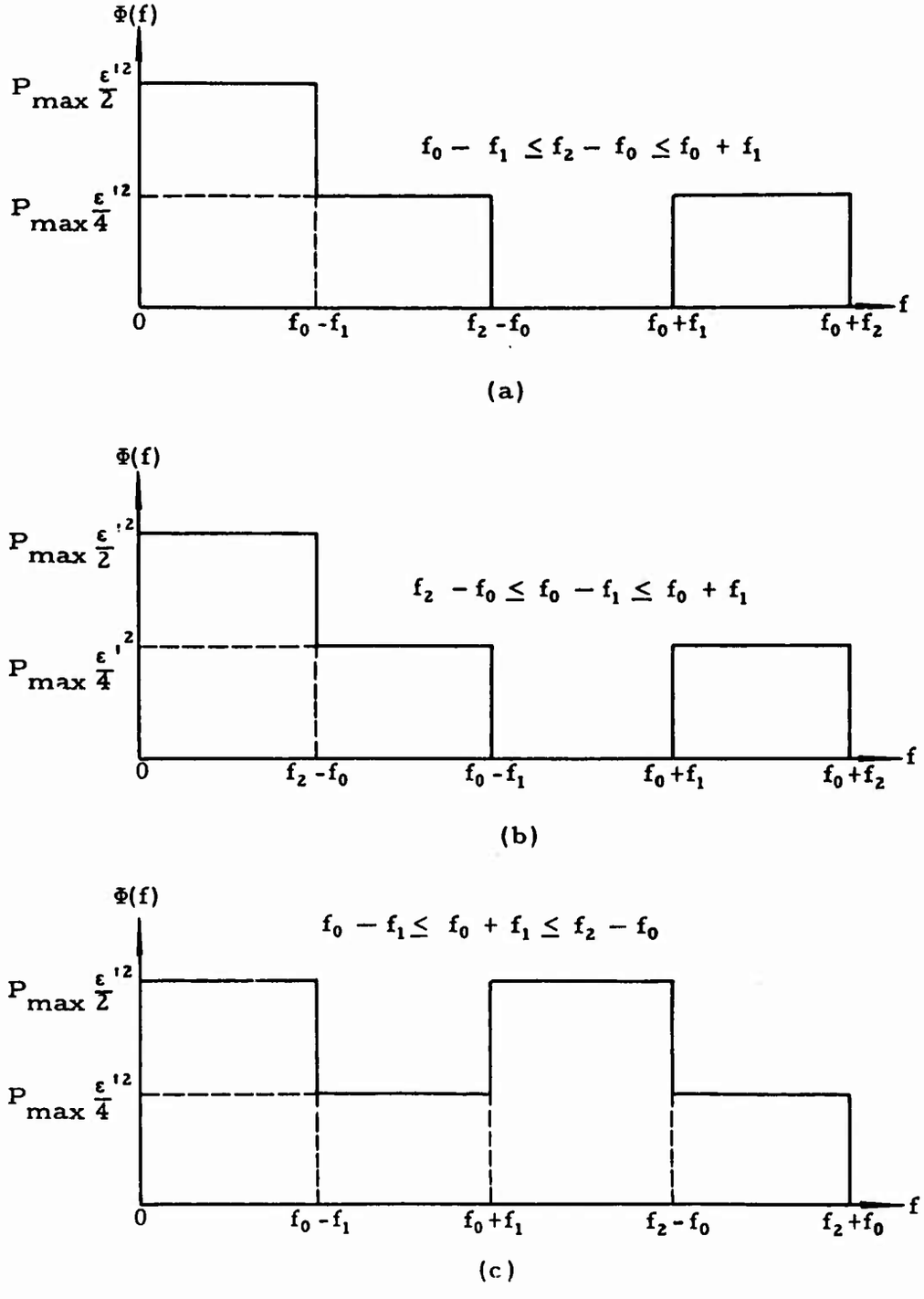

Figure 5. Power Spectrum after Multiplication (Synchronous Rectification)

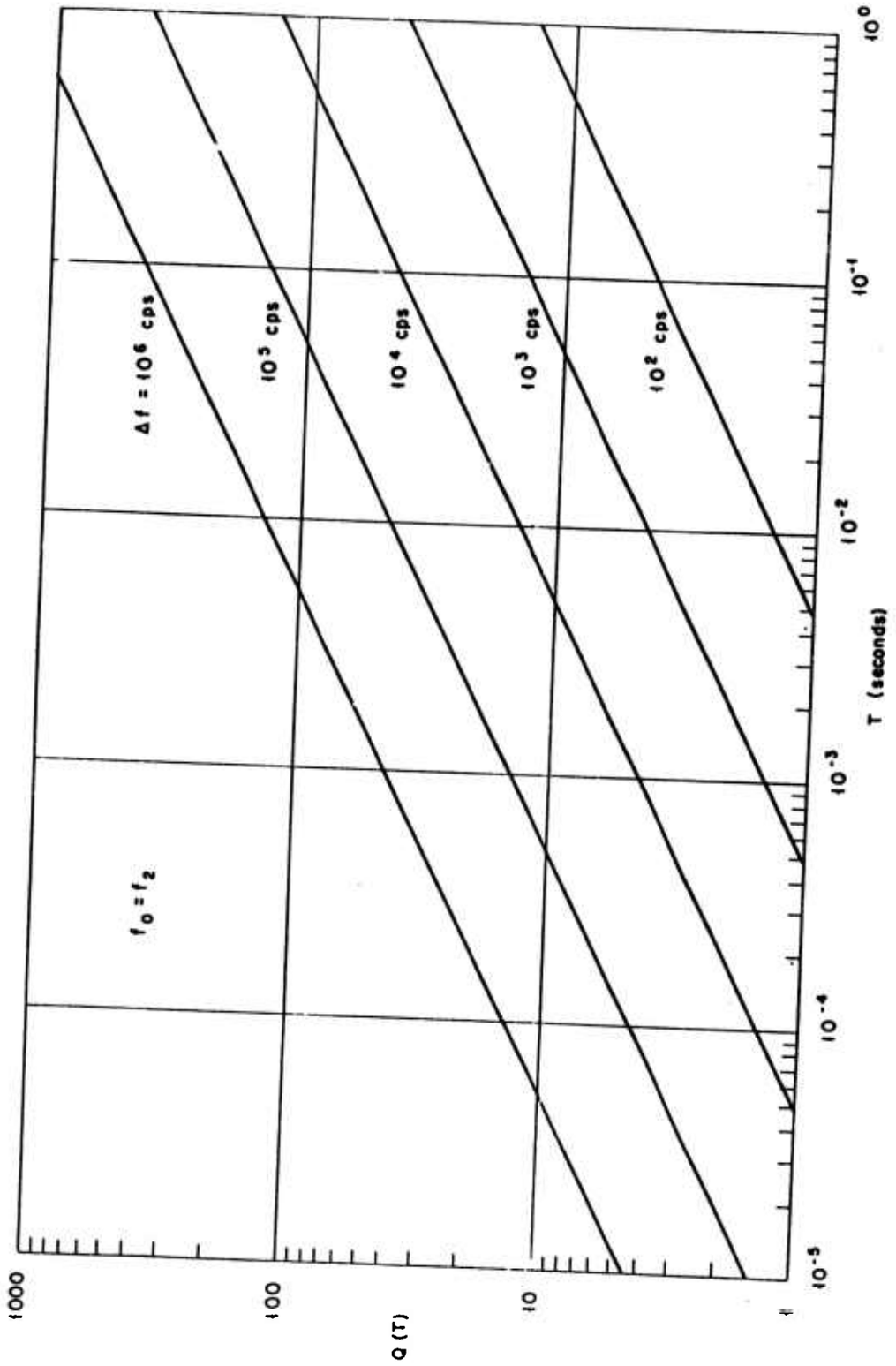

Figure 6. Improvement in Signal-to Noise Ratio by Synchronous Rectification

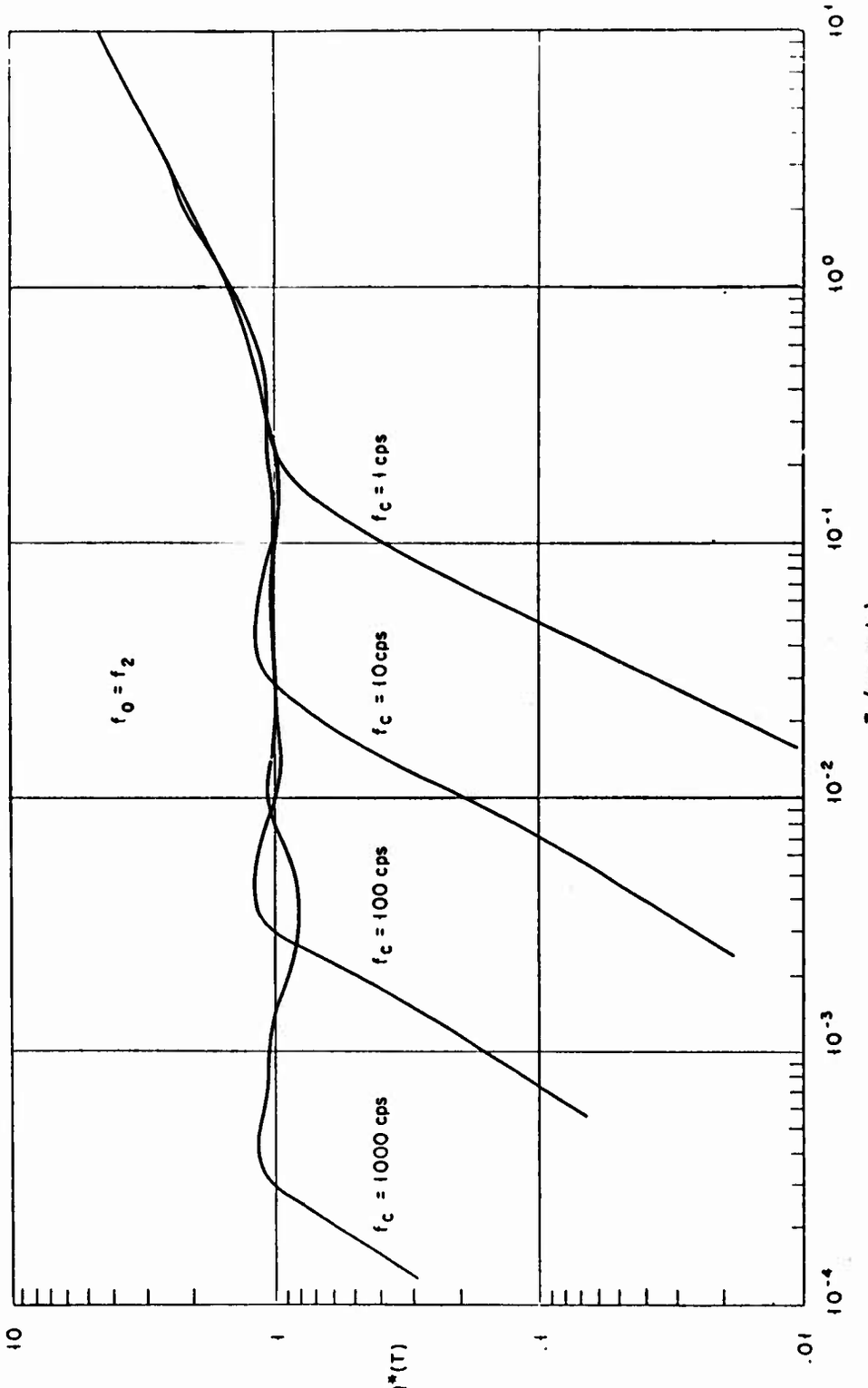

Figure 7. Dependence of Q(T) upon the Position of the Bandwidth in the Frequency Spectrum (Synchronous Rectification)

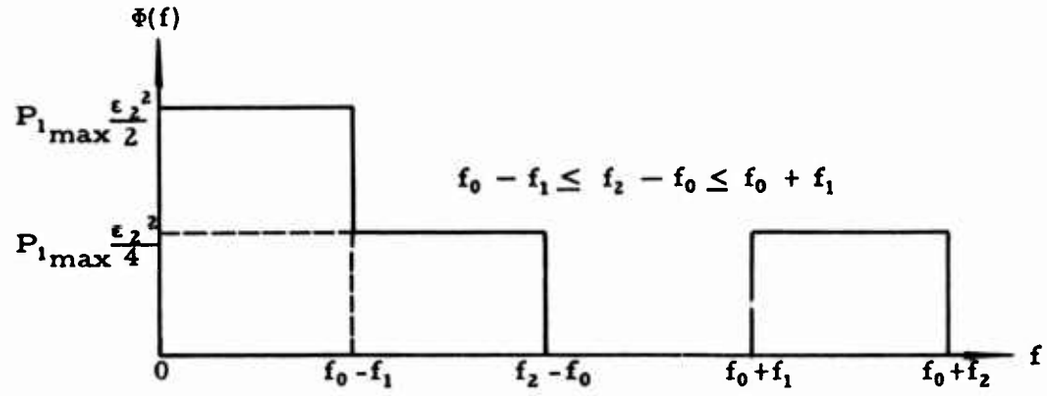

(a)

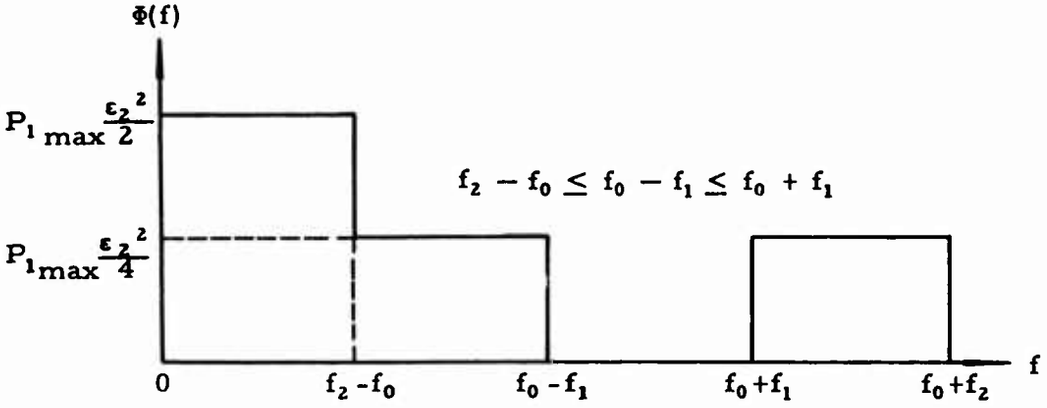

(b)

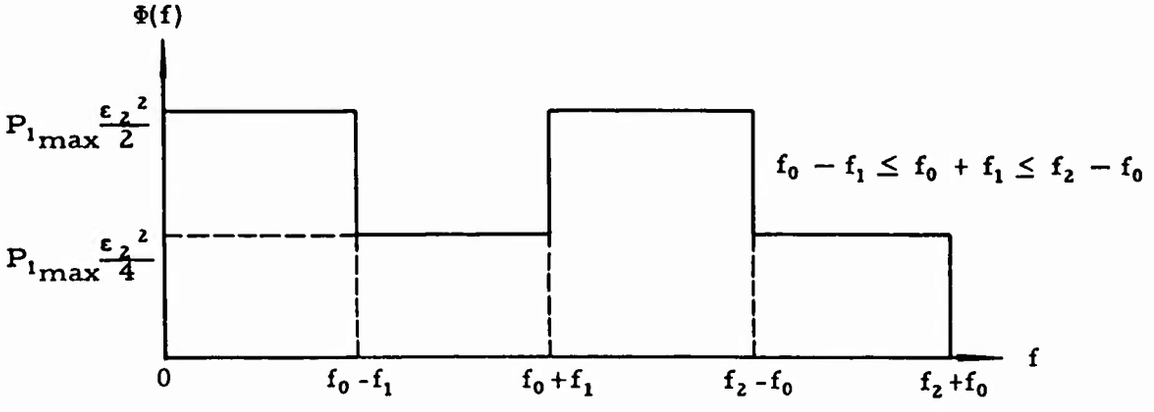

(c)

Figure 8. Power Spectrum of $\Delta N_1(t)$

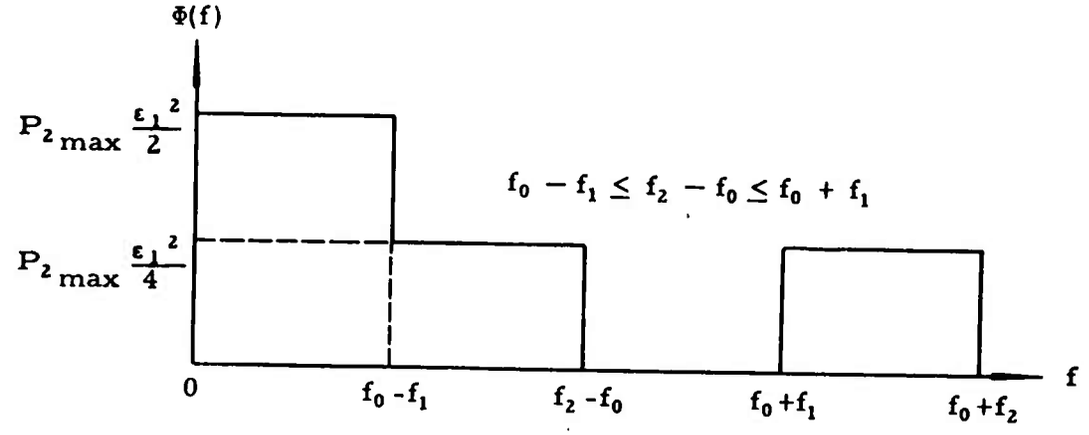

(a)

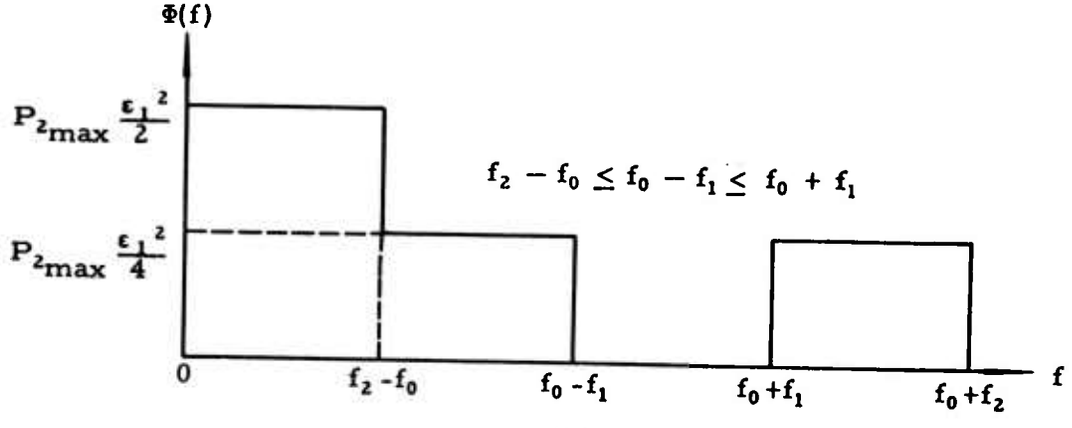

(b)

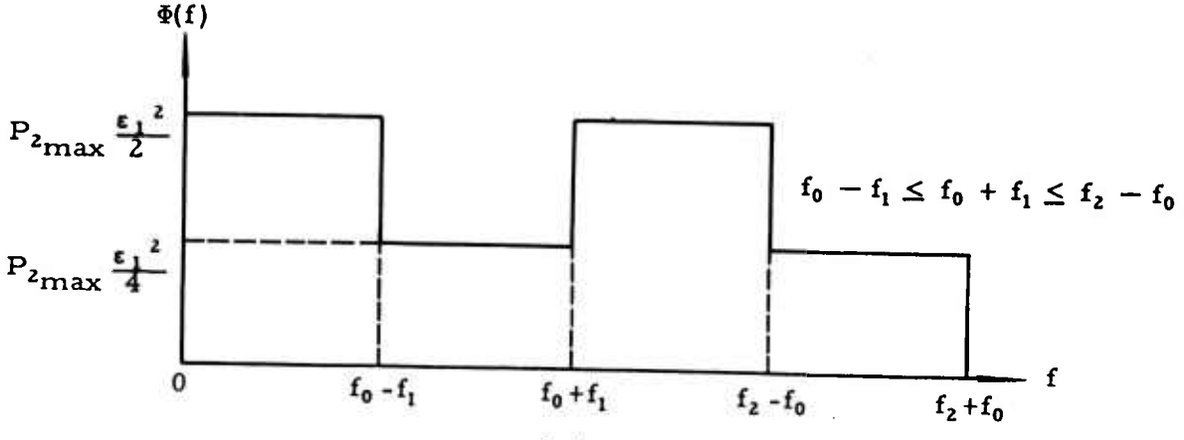

(c)

Figure 9. Power Spectrum of $\Delta N_2(t)$

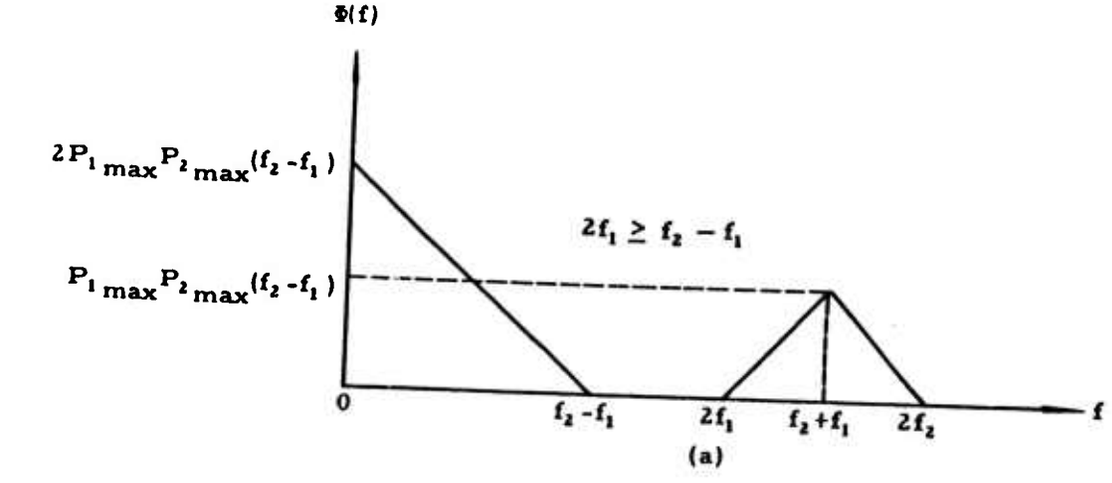

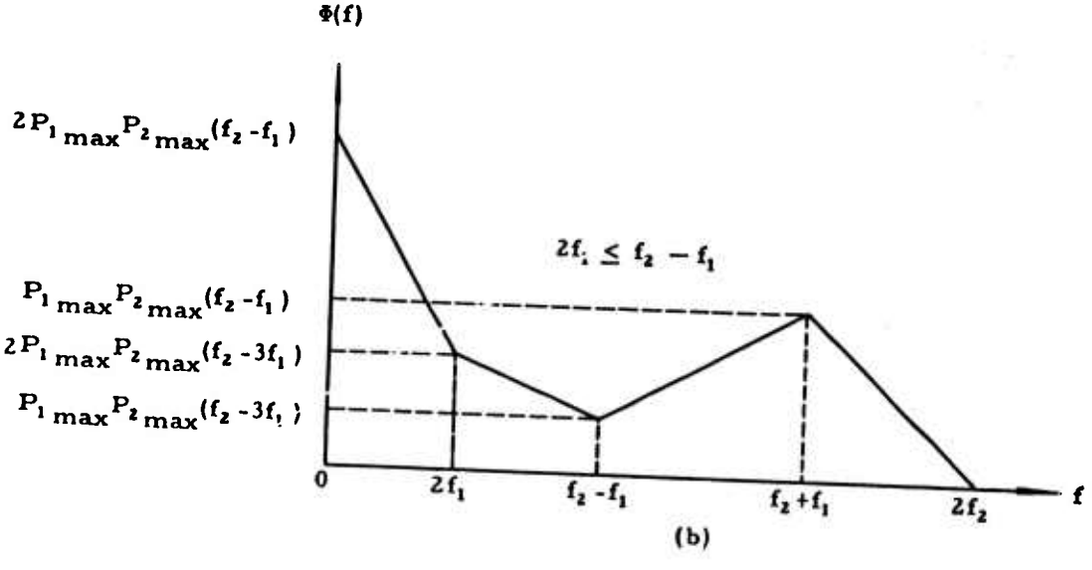

Figure 10. Power Spectrum of ΔN_3 (t)

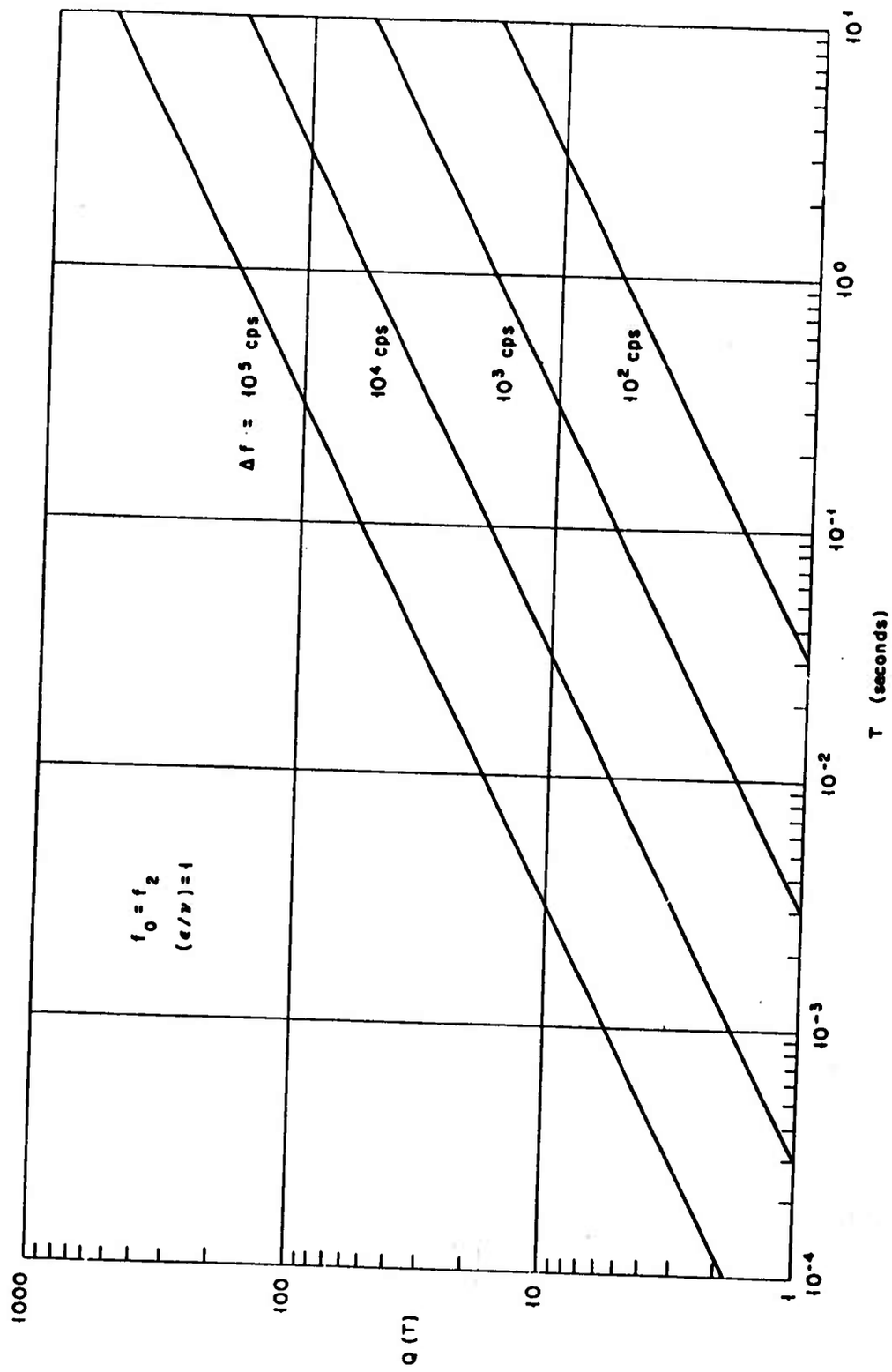

Figure 11. Improvement in Signal-to-Noise Ratio by Two-Detector Cross-Correlation

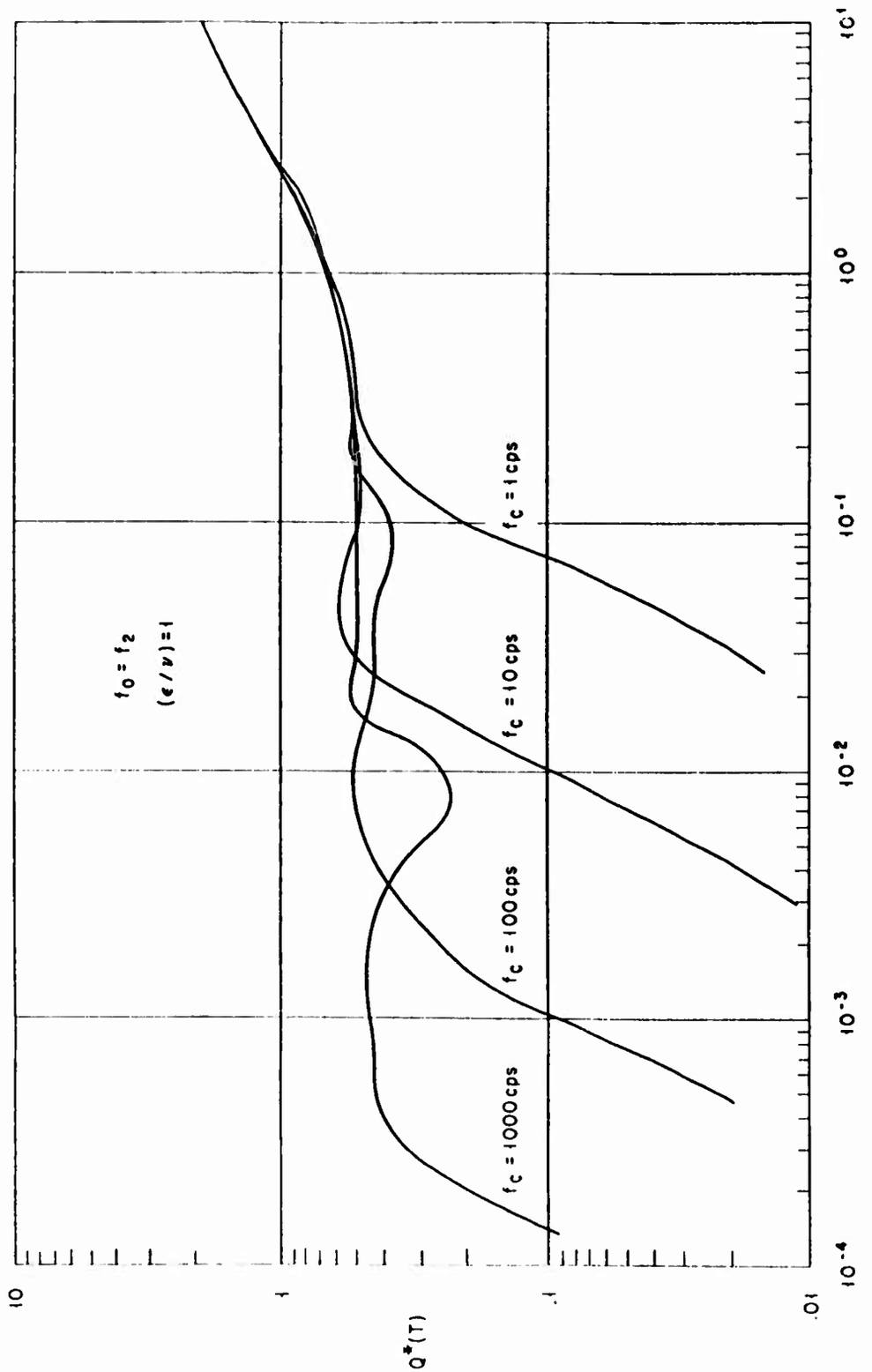

Figure 12. Dependence of Q(T) upon the Position of the Bandwidth in the Frequency Spectrum (Two-Detector Cross-Correlation)

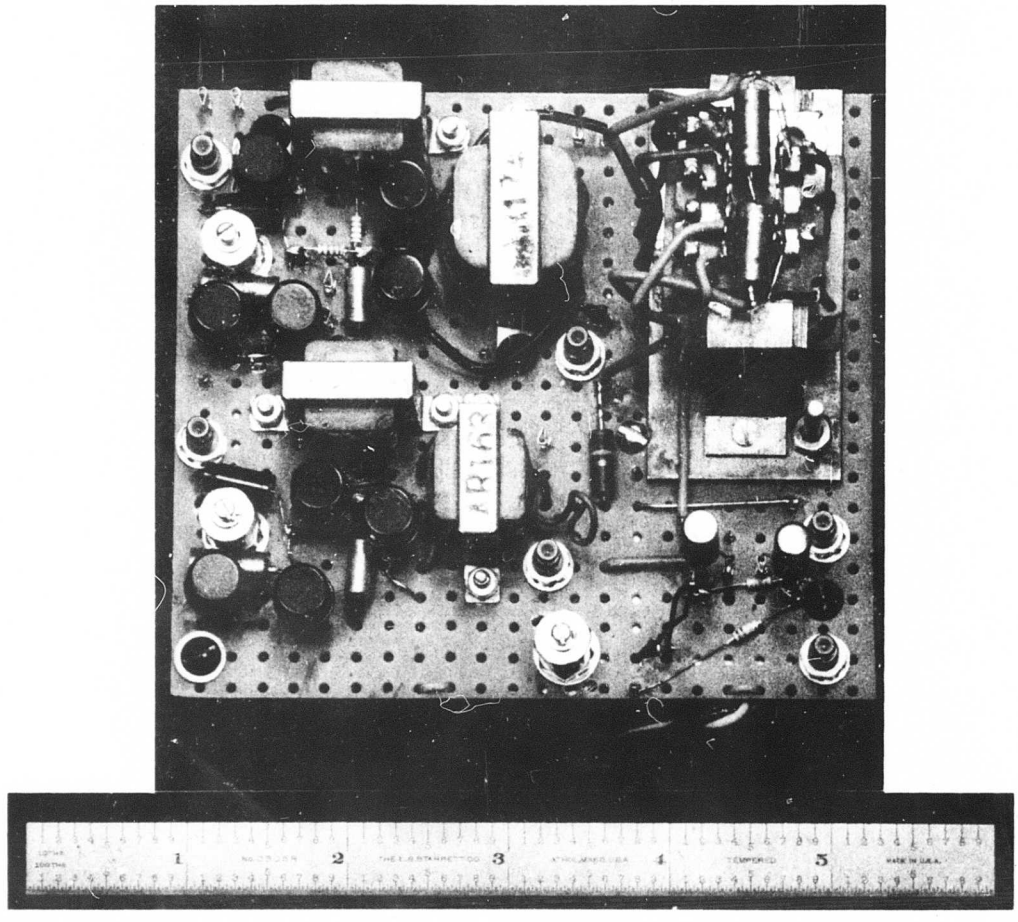

Figure 13. A Miniaturized Correlator Using a Hall-Effect Multiplier and RC Filter

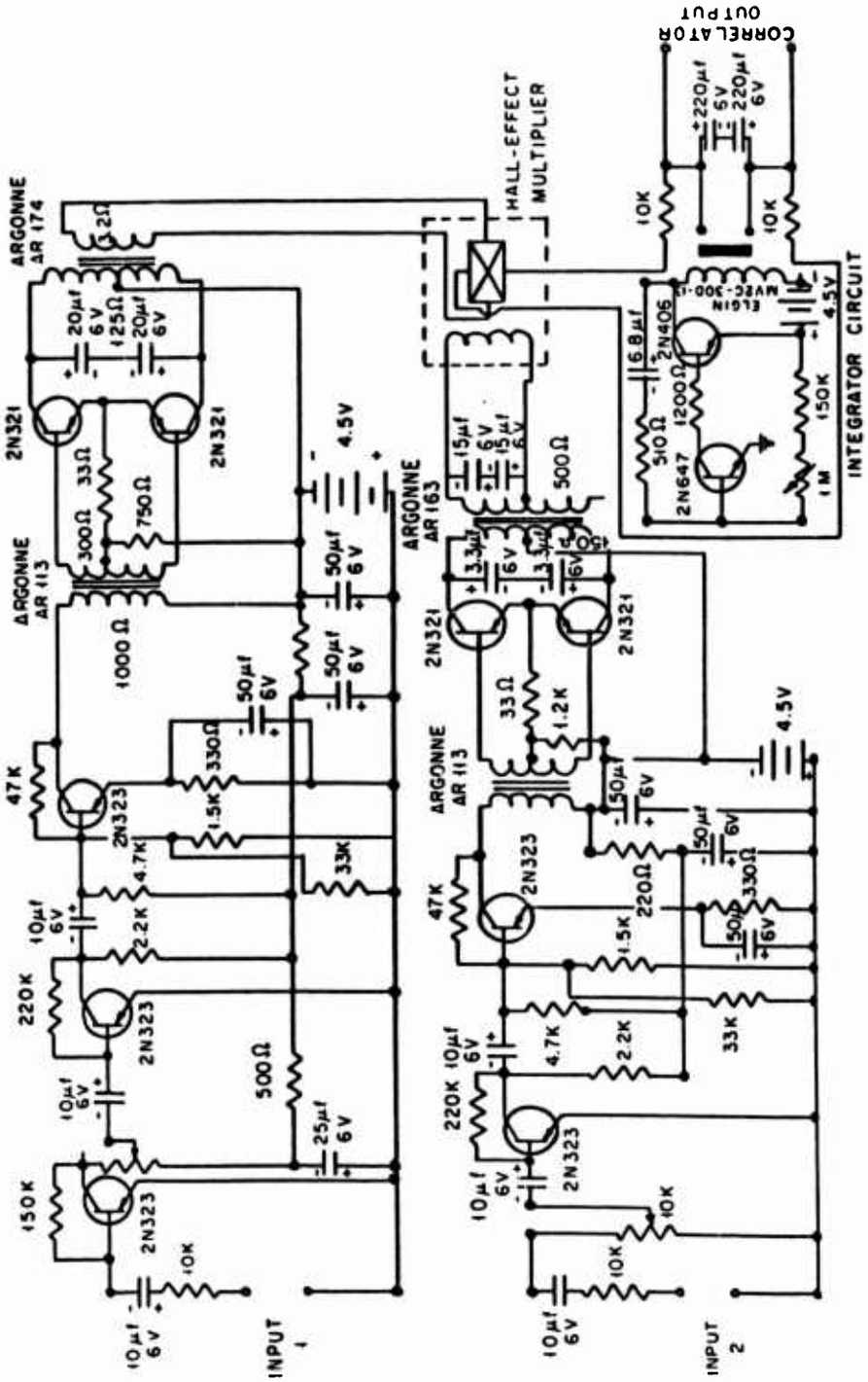

Figure 14. Circuit Diagram of Miniature Correlator and Transistor Amplifiers

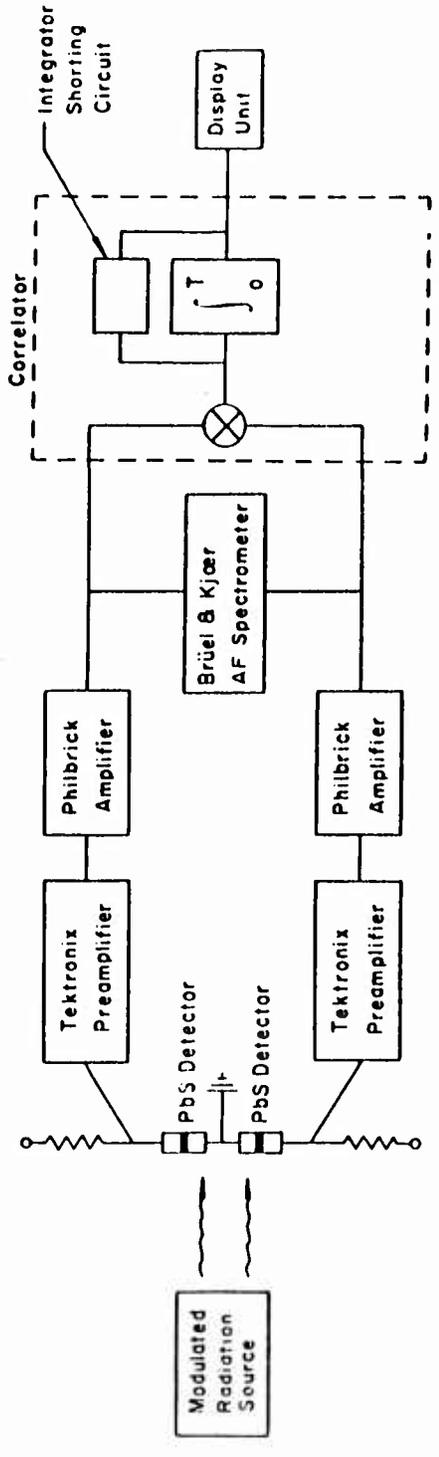

Figure 15. The Experimental System Shown in Schematic Form

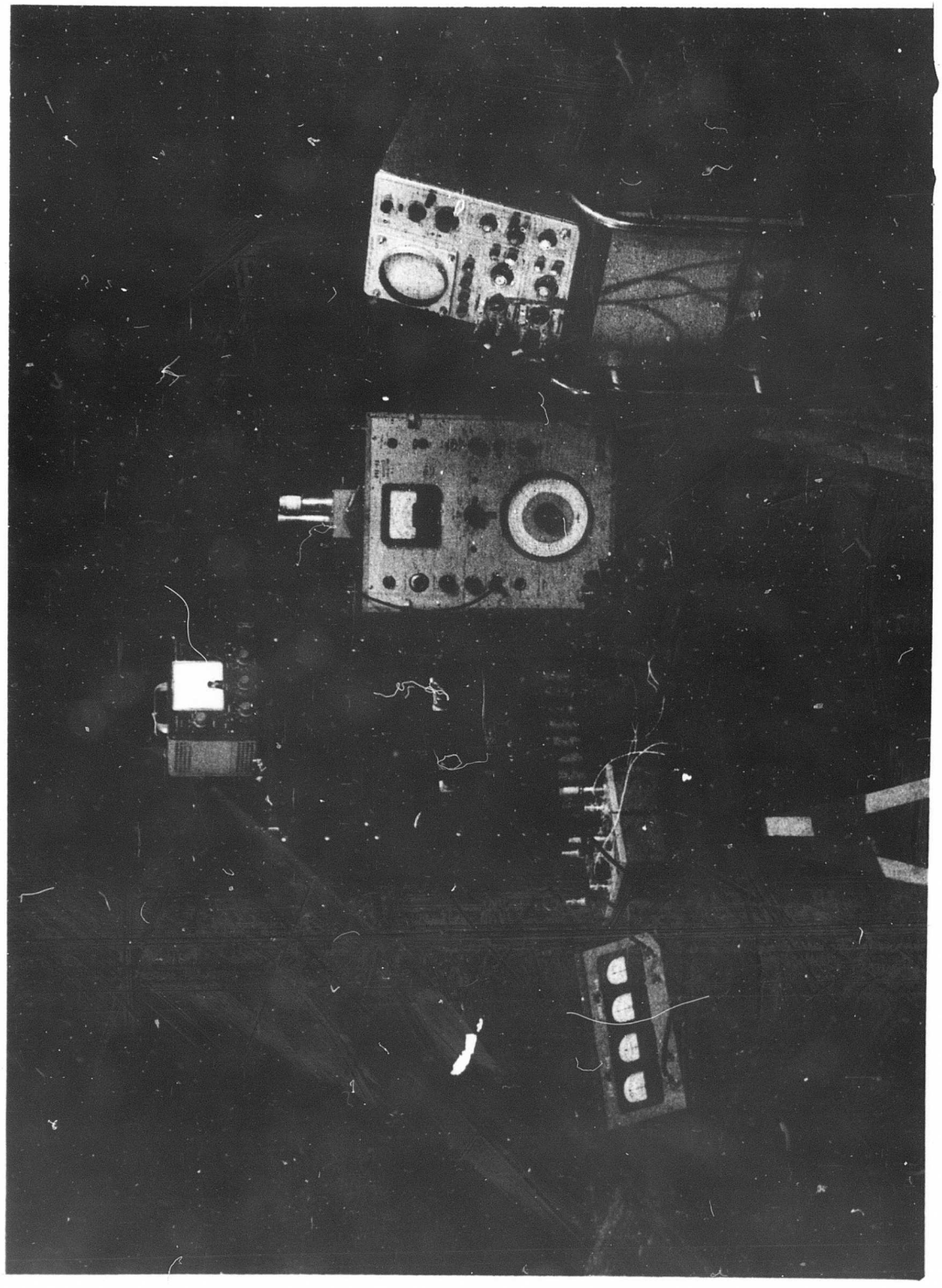

Figure 16. The Experimental System Shown in Pictorial Form

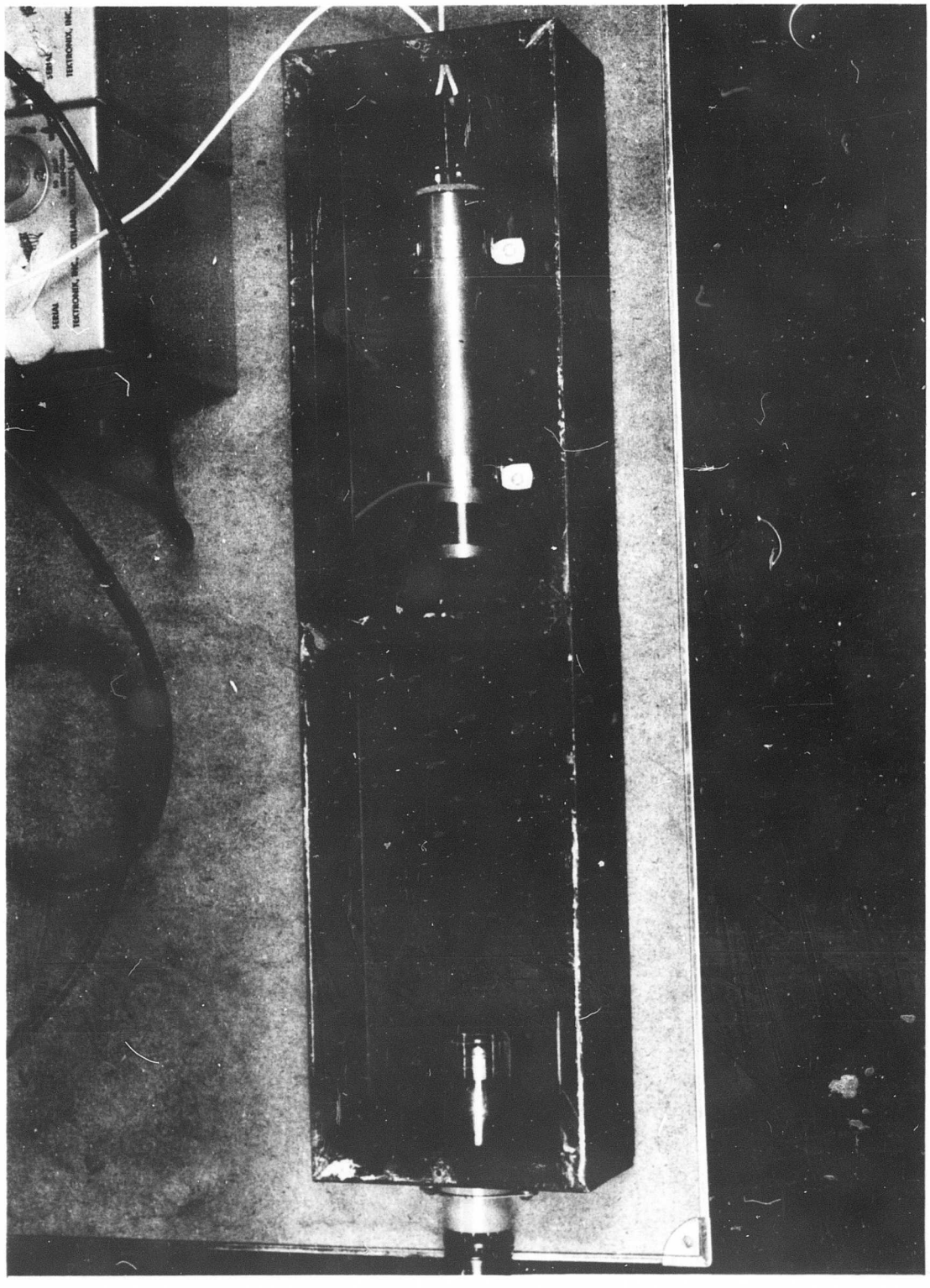

Figure 17. Radiation Source and Detector Assembly

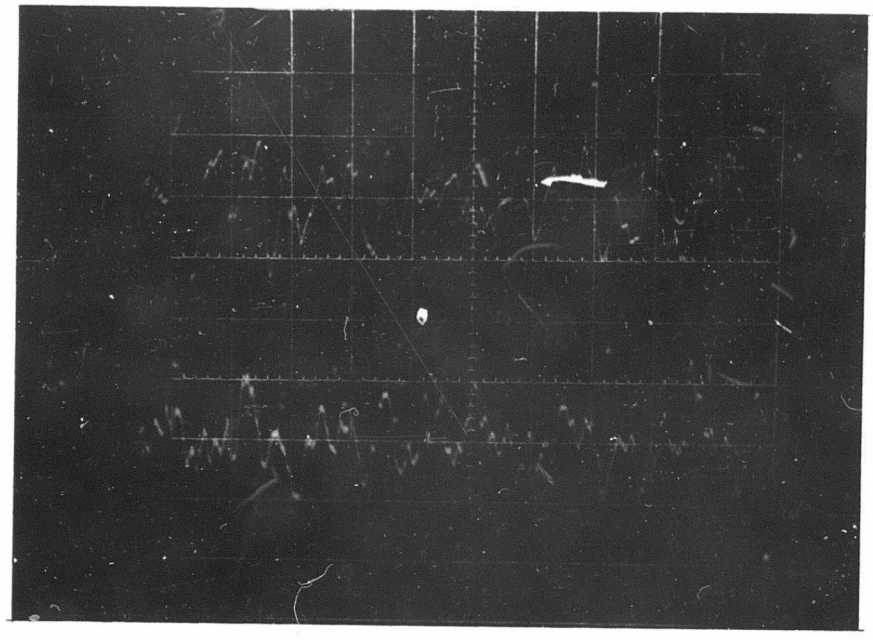

(a) Noise Components Entering Both Channels of the Correlator

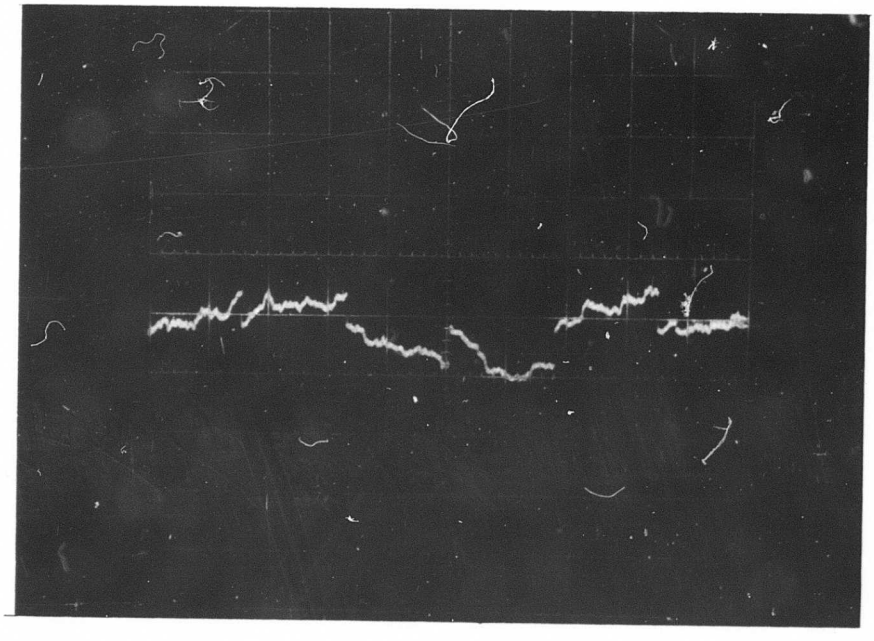

(b) Correlated Noise for Integration Time of about 0.4 sec.

Figure 18

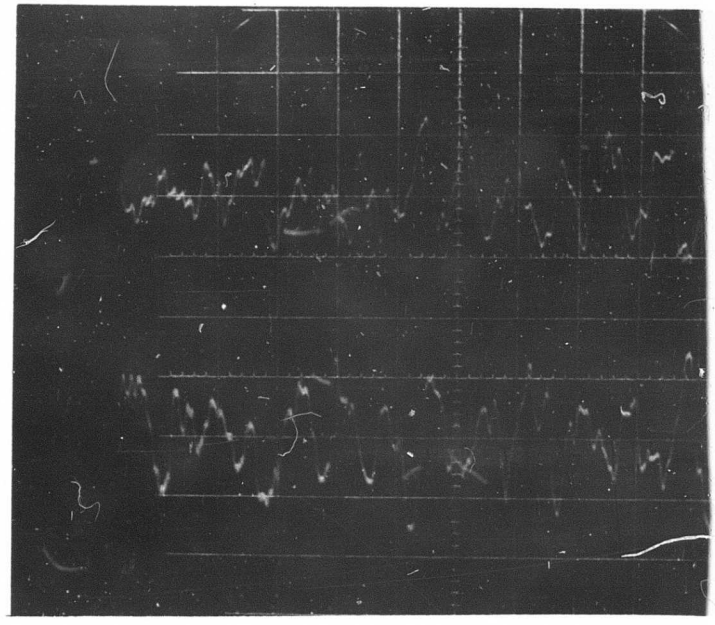

(a) Noise Waveforms with Small Signal Component Ent

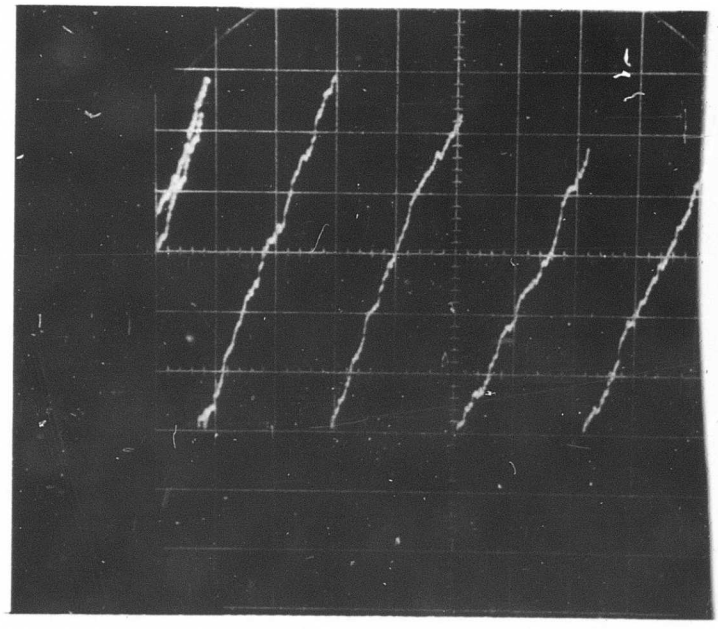

(b) Correlator Output Showing Presence of Signal.

Figure 19

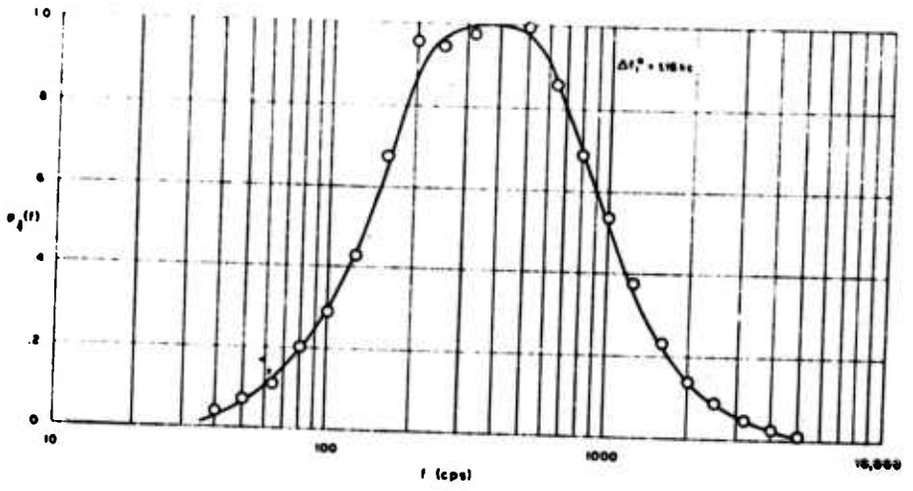

(a)

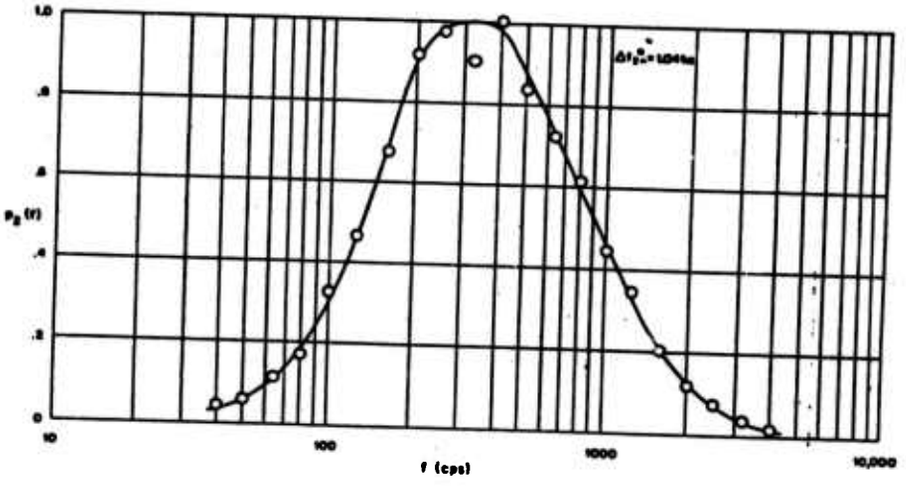

(b)

Figure 20. Power Spectrums of the Noise Entering Each Channel of the Correlator

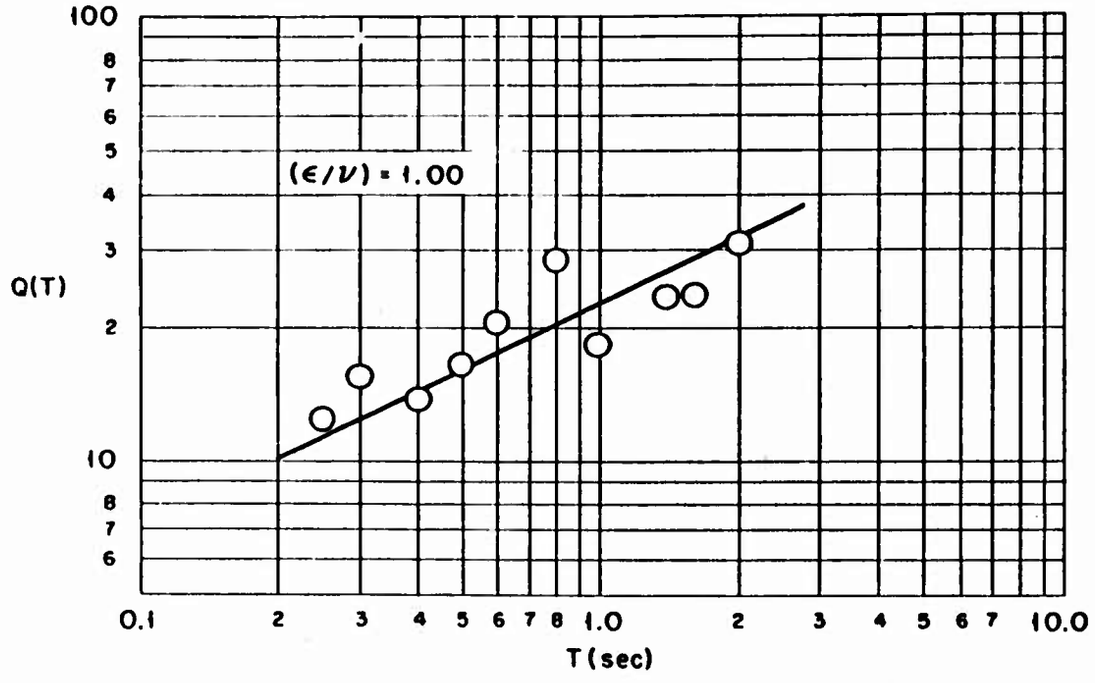

Figure 21. Experimental Data Points and Theoretical Curve for $(\epsilon/\nu) = 1.0$

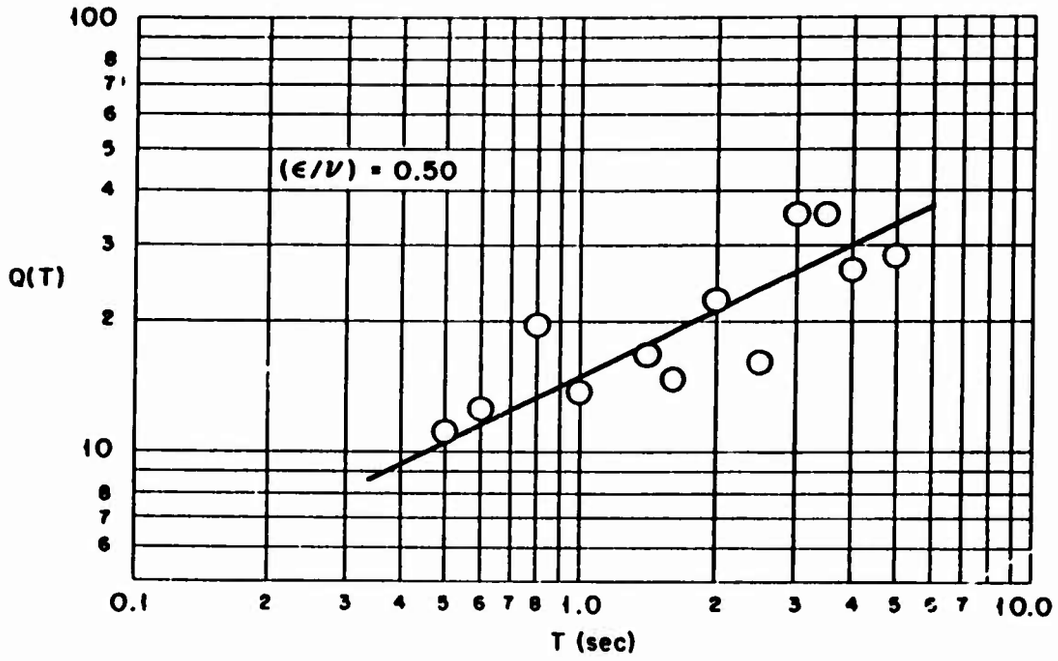

Figure 22. Experimental Data Points and Theoretical Curve for $(\epsilon/\nu) = 0.5$

CONFIDENTIAL